

Characterization of an atypical but widespread type IV secretion system for transfer of the integrative and conjugative element ICE*clc* in *Pseudomonas putida*

Andrea Daveri, Valentina Benigno and Jan Roelof van der Meer ^{*}

Department of Fundamental Microbiology, University of Lausanne, 1015 Lausanne, Switzerland

Received September 08, 2022; Revised December 23, 2022; Editorial Decision January 07, 2023; Accepted January 26, 2023

ABSTRACT

Conjugation of DNA relies on multicomponent protein complexes bridging two bacterial cytoplasmic compartments. Whereas plasmid conjugation systems have been well documented, those of integrative and conjugative elements (ICEs) have remained poorly studied. We characterize here the conjugation system of the ICE*clc* element in *Pseudomonas putida* UWC1 that is a model for a widely distributed family of ICEs. By in frame deletion and complementation, we show the importance on ICE transfer of 22 genes in a 20-kb conserved ICE region. Protein comparisons recognized seven homologs to plasmid type IV secretion system components, another six homologs to frequent accessory proteins, and the rest without detectable counterparts. Stationary phase imaging of *P. putida* ICE*clc* with in-frame fluorescent protein fusions to predicted type IV components showed transfer-competent cell subpopulations with multiple fluorescent foci, largely overlapping in dual-labeled subcomponents, which is suggestive for multiple conjugation complexes per cell. Cross-dependencies between subcomponents in ICE-type IV secretion system assembly were revealed by quantitative foci image analysis in a variety of ICE*clc* mutant backgrounds. In conclusion, the ICE*clc* family presents an evolutionary distinct type IV conjugative system with transfer competent cells specialized in efficient transfer.

INTRODUCTION

Bacterial conjugation is widely appreciated for its importance to horizontal gene distribution and consequent facilitation of adaptation to new selective conditions. Conjugation is mostly attributed to plasmid DNA, but more recently, integrative and conjugative elements (ICEs) have been recognized as additional widespread conjugative vehi-

cles, which, however, are mostly ‘hidden’ (inserted) within the bacterial genome (1–5). ICEs combine both phage-like and plasmid properties. Like temperate phages, they remain mostly integrated in their host genome, and occasionally excise. In contrast to lysogenic phages, excised ICEs spread by conjugation to a new cell, where they re-integrate in the host’s chromosome (Figure 1A). Expression of the ICE excision and conjugation functions is silent in the integrated state, being subject to complex, multi-layered regulatory control that varies across different ICEs (6–8). Various physiological and external cues can lead to activation of ICE transfer (6,8,9). Particularly for the model ICE*clc* of *Pseudomonas knackmussii* B13 (see below), activation only occurs in a subpopulation of transfer competent (tc) cells, and only these cells are the ones that can excise, replicate and conjugate the ICE (9–11).

Most known ICEs have a mosaic ‘modular’ genetic structure, being composed of syntenic conserved gene regions coding for core mobility functions, interspersed with highly variable gene content that can provide adaptive benefits to the host (1,3,5). Different ICE families have been recognized, based on their evolutionary history and relatedness of the different conserved modules (2). Particularly, conserved components of the conjugation machinery, such as the VirB4 and VirD4 ATPases of the Type IV secretion system (T4SS) have been used for the classification (12,13). Based on this, Guglielmini and coworkers proposed eight phylogenetic clades, covering mating pair formation (MPF) systems from both ICEs and plasmids (14). In particular, the MPF_G clade is unique for conjugative systems of ICEs, and has so far not been well-characterized (14). The only studied MPF_G-class member is ICE*Hin1056* of *Haemophilus influenzae*, which non-exhaustively identified a number of T4SS components important for pilus biogenesis (15).

The aim of the current work was to better characterize the MPF_G clade conjugative system from the ICE*clc* element and to uncover features distinct from other (plasmid) MPF systems that might point to specific transfer selection. ICE*clc* is 103 kb long and contains genes encoding for metabolism of 3-chlorocatechol and 2-aminophenol

^{*}To whom correspondence should be addressed. Tel: +41 21 6925630; Email: janroelof.vandermeer@unil.ch

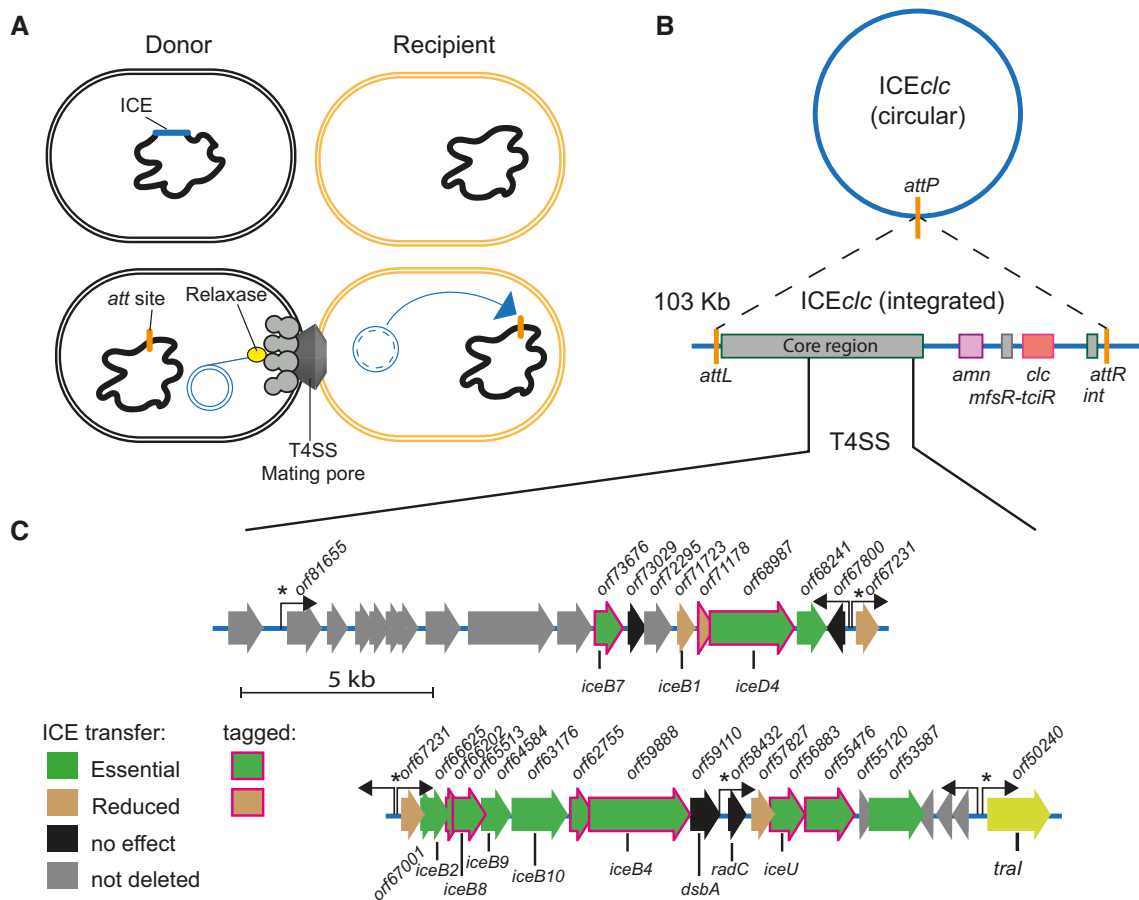


Figure 1. The ICEclc lifestyle. (A) Schematic representation of ICEclc transfer from an integrated state (dark blue) to the excised form (double blue circle) that is conjugated through a type IV secretion system (T4SS) mating pore into a recipient cell (yellow), where integration can occur (blue arrow). (B) Schematic structure of ICEclc with its excised circular form recombined at the *attP* site and the integrated state between *attL* and *attR*. Conserved core region shared with other ICEclc family members is schematically indicated, as well as are key features of ICEclc (*int*, integrase gene; *mfsR-tciR*, regulators; *amn* and *clc*, metabolic pathway gene clusters). (C) Detailed map of the conjugative gene region of ICEclc. Genes and their orientation are represented by colored arrows, with their original *orf* designation (as in GenBank AJ617740.2) described above and the deduced relevant gene names below (gene names follow analogous designation as in the *vir* system). Filled colors correspond to transfer effects as in the colored legend (see Figure 2), whereas magenta arrow outlines point to those components tagged with translational fusions for epifluorescence microscopy. Hooked arrows indicate known promoters; an asterisk pointing to those being active only in transfer competent cells as shown in Ref. (21).

(Figure 1B). It is present in two identical copies in the *P. knackmussii* B13 genome at the 3' end of *tRNA^{Gly}* genes (16,17) and can be conjugated to *Pseudomonas putida* where it maintains a single integrated copy. The ICEclc core region is highly conserved among a wide range of putative ICEs detected in genomes of Beta- and Gammaproteobacteria (7,17). Transfer only occurs from tc cells, that appear in 3–5% of the stationary phase population, notably after growth on 3-chlorobenzoate (9,18). After its excision, the ICEclc molecule can replicate to up to 7 copies in its host tc cell, which may contribute to more effective and multi-recipient transfer (11). Transfer of ICEclc is dependent on the TraI relaxase (Figure 1C), which nicks the DNA at either one of two origins of transfer (*oriT*) (19), and is assumed to guide the single-stranded ICE-DNA molecule to the mating pore.

In order to characterize the components of the ICEclc conjugative system, we deployed a combination of genetic dissection, regular and high resolution epifluorescence microscopy and bioinformatics. We focused on a region on

ICEclc that was previously suggested to locate the genes for its conjugative system (Figure 1C) (20). Out of the 24 genes present in the locus, we seamlessly deleted 22 by double recombination in a *P. putida* ICEclc host background, and complemented each deletion individually *in trans* by a mini-Tn5 delivered single copy wild-type gene, expressed under control of the native ICE promoter upstream of the *orf67231* gene (Figure 1C), which is active only in tc cells (21). The effects of gene deletion and complementation on ICE transfer were quantified from isogenic *P. putida* ICEclc donor-recipient matings. Protein structures were predicted from the genes in this ICE region using AlphaFold2 (22) and Phyre2 (23), and compared to the known protein structure databases to find potential homologs. This analysis was complemented by amino acid similarity searches to archetype T4SS components. Finally, a subset of nine identified components of the ICEclc conjugative machinery was expressed as in-frame fluorescent protein fusions from their native location to study their cellular localization in *P. putida* ICEclc wild-type or mutant backgrounds, and all

fusion proteins were verified for functional ICE transfer. Our results indicate that the ICE*clc* conjugation machinery is a very distant T4SS, with several functionally analogous components to the F-plasmid system of *Escherichia coli* (24), the *Agrobacterium tumefaciens* Vir system (25) or the Dot/Icm system of *Legionella pneumophila* (26,27), but with a number of unique other components important for its transfer.

MATERIALS AND METHODS

Biological resources, reagents and growth conditions

Escherichia coli DH5 α λ pir was used for cloning of ICE*clc* genes and plasmid amplification, and was grown at 37°C on Luria-Bertani (LB) liquid or agar-solidified broth. *P. putida* UWC1-ICE*clc*::lacO_{array} was used as host of the ICE, carrying a single copy ICE*clc* integrated at the tRNA^{Gly}-5 gene (11). The lacO_{array} modification was introduced in the *amnB* gene of the ICE with the purpose to follow single-copy ICE-DNA transfer, if needed (11). *P. putida* UWC1 Tn7 P_{BAD}lacI-*cfp* or UWC1 Tn7 P_{tac}-mCherry were used as recipient strains for mating experiments. *P. putida* was cultured at 30°C either on LB, on nutrient agar (Oxoid) or on minimal medium (MM, type 21C (28)). MM was supplemented with either 5 mM succinate or 3 mM 3-chlorobenzoate (3-CBA) as sole carbon source. Both *E. coli* and *P. putida* were cultured aerobically in shaking flasks. Where necessary for plasmid maintenance or for selection of genomic constructs, antibiotics were added at the following concentrations: kanamycin (Km, 50 μ g ml⁻¹), ampicillin (Amp, 100 μ g ml⁻¹ for *E. coli*, 500 μ g ml⁻¹ for *P. putida*), tetracycline (Tc, 20 μ g ml⁻¹ for *E. coli*, 50 μ g ml⁻¹ for *P. putida*), or gentamycin (Gm, 20 μ g ml⁻¹, 10 μ g ml⁻¹ in MM). The following supplements were added for screening or promoter induction (see below): 5-bromo-4-chloro-3-indolyl- β -D-galactopyranoside (X-Gal; 20 μ g ml⁻¹), isopropyl- β -D-1-thiogalactopyranoside (IPTG, 0.5 mM), or *m*-toluate (15 mM). All produced strains are listed in Supplementary table S1.

DNA manipulations

DNA manipulations followed standard procedures or as indicated by the reagent supplier. Plasmids were purified from *E. coli* DH5 α λ pir using NucleoSpin Plasmid kits (Macherey-Nagel, Duren, Germany). Oligonucleotide primers were purchased from SigmaAldrich. PCR amplicons and digested fragments were purified using NucleoSpin Gel and PCR Clean-up kits (Macherey-Nagel). Clones were initially screened by PCR on resuspended individual colonies in a GoTaq® G2 green master mix (20 μ l, Promega, Madison, United States). Plasmid fragments were assembled using the ClonExpress II One Step Cloning Kit (Vazyme, Nanjing, China), digesting the plasmid backbone with appropriate restriction enzymes (New England Biolabs, Ipswich, United States), and mixing with insert-DNA. All of the constructed plasmid inserts were sequenced prior to further use in *P. putida*, to verify their correctness, using the ICE*clc* sequence as a reference (29) (GenBank AJ617740.2). Plasmids are listed in Supplementary table S2.

Chromosomal gene knockouts and complementations

Seamless in-frame deletions of ICE*clc* genes were created using double recombination with marker counterselection (30). Up- and downstream regions (~800 bp) of the target gene were PCR amplified using Q5 high fidelity polymerase (New England BioLabs) and primers as detailed in Supplementary table S3, and subsequently cloned into the suicide vector pEMG (30). Purified plasmids (300–500 ng) were electroporated into *P. putida* UWC1-ICE*clc*::lacO_{array} as described previously (19). Single recombinants were selected on plates with Km, and colonies were verified by PCR for integration of the suicide vector. Single recombinants were then cultured and transformed with 50 ng of purified plasmid pSW (30). Transformants were cultured and induced by addition of 15 mM *m*-toluate (Honeywell Fluka™) for 16 h, to express the I-*SceI* nuclease and force chromosomal repair, after which culture dilutions were spread on LB plates. Candidate colonies were again verified by PCR for the success of the double recombination and the deletion genotype. Successful clones were then cultured in absence of antibiotics to segregate out pSW, and stored at –80°C with 15% v/v glycerol.

Deleted genes on ICE*clc* were complemented by individual or combinations of the cognate gene(s), placed *in trans* in single-copy on the *P. putida* chromosome using mini-Tn5 delivery (31). ICE*clc* genes for complementation were amplified using Q5 high-fidelity DNA polymerase (New England BioLabs) and primers as in Supplementary table S3, and then brought under control of the native wild-type ICE*clc* promoter P₆₇₂₃₁ that is active only in tc cells (21). The 360-bp P₆₇₂₃₁-promoter region was amplified with primers containing appropriate restriction sites for cloning into the mini-Tn5 delivery vector pBAM (31) and overhangs to allow assembly. Assembled DNA mixtures were transformed by heat-shock into *E. coli* DH5 α λ pir for propagation and plasmid DNA purification. Purified plasmids were sequenced to verify the cloned insert, and electroporated into the corresponding *P. putida* ICE*clc* gene deletion strain. Integrants were selected for antibiotic resistance from the mini-Tn5 delivered construct and verified by PCR, after which three clones with potentially different integration positions of the complementation insert were frozen at –80°C for further analysis.

Fluorescent protein fusions

The same strategy used to produce gene deletions was employed for translationally fusing fluorescent protein tags (mCherry or sfGFP) at the N- or C-terminal end of target ICE*clc* conjugative system proteins. In case of N-terminal fusion the open reading frame of the fluorescent protein was inserted after the signal sequence if present (e.g. *orf62755*), otherwise following the start codon (e.g. *iceB8*), followed by a short linker peptide as in (32). In case of C-terminal fusion the linker and the fluorescent protein were inserted before the stop codon of the target gene. In the eventuality of overlap between the translation stop and start of two consecutive genes, the insertion was performed in such a way that the ribosome binding site of the following gene

remained intact. Primers used for the amplification of the homology regions and fluorescent proteins are listed in Supplementary table S3. Cognate ICE $_{c}$ -genes were replaced with the fluorescently-tagged version directly on wild-type integrated ICE $_{c}$ in *P. putida* or on ICE $_{c}$ carrying additional deletions for conjugative components. *P. putida* without ICE $_{c}$ was used as control for fluorescent protein auto-aggregation, and transformed with relevant mini-Tn5 constructs and plasmids pME-*bisR* or pME-*bisDC* expressing two known transcriptional regulators involved in ICE $_{c}$ activation to induce the P₆₇₂₃₁-promoter in all cells (7). *P. putida* codon-optimized coding sequences (JCat tool (33)) for mCherry and sfGFP were synthesized by ThermoFisher (Waltham, USA).

Protein homology assignments

Homology and functional predictions focused on ICE $_{c}$ genes in the conserved presumed conjugative gene region (gene designations *orf53587*–*orf73676*, as defined in AJ617740.2, Figure 1C). To avoid finding numerous spurious hits to highly homologous ICE genes in other bacterial genomes, we first compared the translated amino acid sequences from individual ICE $_{c}$ genes to each of the known components of the classical ‘Vir’ T4SS from *A. tumefaciens* (NZ_CP029048.1) by EMBOSS *needle* alignment across the full protein length. Next, we identified any conserved domains by BLASTp (34), Phyre2 (23), pfam (35), or Dali (36), and used TMHMM (37) and SignalP (38) to predict the presence of transmembrane domains and signal peptides. Finally, we used AlphaFold2 (22) to predict structures for each of the presumed ICE $_{c}$ conjugative components (using standard settings on the web server platform https://colab.research.google.com/github/sokrypton/ColabFold/blob/main/beta/AlphaFold2_advanced.ipynb), and then compared the highest ranked derived .pdb structure prediction in PDBeFold (39) with the PDB database to find potential structural analogs. PDBeFold analyses were carried out with default parameter settings.

ICE $_{c}$ transfer experiments

ICE $_{c}$ transfer was quantified from binary mating experiments. As donors we tested *P. putida* carrying ICE $_{c}$ wild-type, or ICE $_{c}$ with an inserted *lacO*_{array} (11), ICE $_{c}$ gene deletion variants and the various complemented strains, as well as fluorescent protein fusion variants. As recipient we used isogenic but ICE $_{c}$ -free *P. putida* UWC1 carrying a chromosomally integrated Gm resistance (Supplementary table S1). Donors and recipient were freshly plated from –80°C stocks on LB agar plates with appropriate antibiotics and grown for 16 h. Three separate clones (donors) and a single colony (recipient) were picked and inoculated each in 10 ml LB with antibiotics. These individual pre-cultures were grown for 24 h, after which a volume of 40 μ l was transferred into 8 ml MM with 3 mM 3-CBA (donors) or 5 mM succinate (recipient) as the sole carbon sources, without antibiotics. After 48 h (donor) and 24 h (recipient) of growth the culture turbidities were measured (OD₆₀₀), and

recipient and donor cultures were mixed together in new vials in a 2:1 ratio (OD/OD), respectively, and to a final volume of 1 ml. Donor and recipient cultures alone served as controls for the appearance of background growth on selective plates.

Donor-recipient cell mixtures were centrifuged at 13 000 rpm (Thermo Scientific Fresco™ 21 Microcentrifuge) for 2 min, after which the supernatant was discarded and the cell pellet was resuspended in 1 ml of sterile MM (without carbon source). The suspension was centrifuged as before and cell pellets were now resuspended in 20 μ l of MM. The suspension was transferred on top of a 0.2- μ m, 25 mm ϕ cellulose acetate filter (Huberlab, Aesch, Switzerland), that had been placed on a MM agar plate with 0.5 mM 3-CBA. Matings were incubated at 30°C for 48 h, after which cells were washed from the filters with 1 ml MM. Cell suspensions were tenfold serially diluted and 5 μ l aliquots of every dilution were dropped and dried on MM-agar with 3 mM 3-CBA to select for the donor alone, on MM-agar with 5 mM succinate and Gm to select for the recipient, and on MM-agar with 3 mM 3-CBA and Gm to select for the transconjugants. Plates were incubated at 30°C until colonies appeared. ICE $_{c}$ transfer rates were then calculated as the ratio of the number of transconjugant colonies per filter and that of the donor. Transfer rates were normalized across different experiments to that of *P. putida* ICE $_{c}$::*lacO*_{array}, which was used as positive control in all experiments.

Epifluorescence microscopy

Fluorescently labelled *P. putida* ICE $_{c}$ strains were grown for 96 h in liquid MM supplemented with 3 mM 3-CBA to induce the ICE $_{c}$ transfer competence pathway (7). Cells were then transferred on the surface of 1-mm thick 1% MM-agarose patches (ϕ 1 cm) placed upside down on a round microscope slide and enclosed in an imaging chamber (Perfusion Chamber, H. Saur Laborbedarf, Germany) as described (9). Cells were imaged with a Nikon Eclipse Ti-E inverted microscope with a perfect focus system (PFS), pE-100 CoolLED, a Plan Apo λ 100 \times 1.45 oil objective (Nikon) and a Hamamatsu ORCA-Flash4.0 V2 C11440-22CU camera (Hamamatsu, Hamamatsu City, Japan) installed in a controlled temperature room (22°C). sfGFP and mCherry fluorescence were imaged with exposure times of 500 ms and exported as 16-bit .TIF files. Images for display were adjusted to the same level in Adobe Photoshop (v. 2020, Adobe Inc.), downsampled to 8-bit, cropped and saved as 300 dpi.

For improved resolution, samples of the same cell cultures were additionally imaged with a ZEISS LSM 980 Airyscan 2 microscope equipped with ZEN 3.3 software, installed in a controlled temperature room (22°C). Bacterial cells were located on the agarose patches using phase-contrast, after which Z-stacks (Z = 0.17 μ m, 14 layers) of individual cells were acquired in the GFP and/or mCherry channels with an exposure time of 314 ms per layer. Images were processed with the Zeiss Deconvolution algorithm with default settings. Images show a single representative deconvoluted 170-nm Z-slice saved as .TIF file, ‘auto-

toned' in Adobe Photoshop (v. 2020), cropped to the final size and saved as 300 dpi.

Image analysis

Individual *P. putida* cells were segmented on the Nikon 16-bit .TIF phase-contrast images using SuperSegger (40), and the fluorescence intensities, scores, and positions of up to 5 foci in individual cells were extracted. SuperSegger uses 1D-Gaussian fitting on background-normalized and watershed fluorescence cell images to detect foci, as illustrated in Supplementary Figure S1. Subpopulations of tc cells were identified from quantile-quantile plot analysis (41) of the median cell sfGFP or mCherry fluorescent signals. 'Real' and spurious fluorescent foci were distinguished by plotting distributions of the normalized foci intensities among tc and non-tc cell populations, and setting a threshold at which the probability for foci detection in non-tc cells was <1%. Custom made MATLAB scripts were used to extract the following parameters: number of foci per cell, median fluorescence intensity per cell, median top 5% pixel intensity per cell (as proxy for foci intensity), distributions of SuperSegger foci scores (quality of the Gaussian fit) and of Gaussian fit sigma values (as proxy for the apparent foci peak-to-size aspect).

Linear fluorescence profiles were derived from the outer 2-pixel (px) perimeter ('cell envelope') of each identified tc cell using its phase-contrast logical mask, and a further 1-px dilated mask. Profiles were scaled to a median cell perimeter of 50 px for plotting. The 20th percentile fluorescence value was taken as proxy for the cell 'membrane' fluorescence background, from which we calculated the median across all tc cells per replicate ($n = 142\text{--}1996$ cells); which were compared between wild-type fluorescent protein labeled strains and those with gene deletions in ICE*clc*. The standard deviation of the pixel fluorescence values in the two cell perimeters was calculated as second proxy for potential relocation of fluorescent protein from foci to the cell envelope.

Statistical comparisons

ICE*clc* transfer rates were normalized across all experiments to that of *P. putida* ICE*clc*::*lacO*_{array}, which was taken as a control in all individual mating series. Significance of transfer rate decrease was then calculated by pair-wise two-tailed *t*-test comparison of independent biological triplicate matings to that of the wild-type. Subpopulations of tc cells were estimated from quantile-quantile plotting of sfGFP or mCherry fluorescence values with a 95% confidence assumption (41). Differences in foci intensities were tested from pair-wise comparison to their wild-type ICE protein fusion of the median top 5% fluorescence pixel value in biological triplicates (as proxy for the foci intensity), and of the proportion of tc cells without detectable foci (above a normalized foci intensity threshold of 6 for -sfGFP, -mCherry fusions, and 3 for Orf55476-mCherry fusions due to lower background). Median 20th percentiles and median standard deviations of cell envelope pixel fluorescence values were compared between wild-type and mutants in a two-sample equal variance *t*-test.

RESULTS

Function prediction of the genes in the conjugative region of ICE*clc*

In order to better delineate the genes on ICE*clc* important for conjugative transfer and to define their potential functional roles, we focused on the region in between *orf53587* and *orf73676* (Figure 1C) with previously shown low homology to *H. influenzae* ICE*Hin1056* (20). Low amino acid similarities (23–30%) were found in full-length alignments of some ICE*clc* genes and VirB-T4SS components encoded by the Ti plasmid of *A. tumefaciens*, notably, VirD4, VirB1, VirB2, VirB4, VirB8, VirB9 and VirB10 (Table 1). Further structure prediction using AlphaFold2 and comparison with the PDB database suggested that these may be *bona fide* T4SS functional homologs (Table 1, Supplementary figure S2). An additional ICE gene product (Orf73676) showed structural homology to DotD of the Dot/Icm system of *L. pneumophila* and contained a lipoprotein signal peptide (Table 1). DotD is a component of the T4SS outer membrane complex (42) and an analog of VirB7 of the *Xanthomonas citri* T4SS (43). Another gene (*orf56883*) showed domain similarity to TraU (Table 1) of the F-plasmid in *E. coli* (44).

In contrast, the products of the ICE*clc* genes *orf53587*, *orf55476*, *orf62755*, *orf66202* and *orf68241* displayed conserved domains to other hypothetical proteins but without function prediction, nor structural overlap to other known proteins, although with predicted transmembrane helices and/or translocation signals (Table 1). A lipoprotein signal sequence was further predicted for the *orf62755* gene product, suggesting it may be localized in the outer membrane. A further number of genes in this ICE*clc* region code for proteins with detectable functional domains, but unrelated to the T4SS per se (e.g. a RadC DNA repair domain in Orf58432, Table 1). Several proteins have predicted functional domains related to cysteine modifications (i.e. *orf57827* disulfide oxidoreductase, *orf59110* protein disulphide isomerase, *orf71178* thioredoxin oxidoreductase, *orf72295* disulfide oxidoreductase), suggesting their implication in post-translational protein modifications. Some ICE-encoded proteins showed structural similarities with multicomponent ring-like membrane complexes, such as *orf67001* and *orf67231* (Table 1, Supplementary figure S2), suggesting they may be forming multi-subunit structures in the inner membrane. Finally, the *orf73029* gene product showed structural similarity to a protein involved in pilus biogenesis (Table 1). Although none of the software used showed any significant similarities for the *orf55476* gene product, previous alignments (20) had pointed to low amino acid similarity (41%) with a proposed PilT homolog of ICE*Hin1056* (15). The *orf55476* protein was further predicted to carry a translocation signal peptide (Table 1). Therefore, it may encode a PilT-like ATPase of the ICE*clc* conjugative machinery, involved in pilus de-polymerization (45).

The sequence and structural homology searches thus suggested the following protein subassemblies for the ICE*clc* T4SS (Supplementary figure S2), which, whenever possible, we propose to rename analogous to the Vir-nomenclature (e.g. *orf59888* becomes *iceB4* in analogy to *virB4*,

Table 1. Sequence and structural homology predictions of genes in the ICE c conjugative transfer region

ICE c gene designation ^a	Length (aa)	Archetype T4SS ^b	Similarity %/gaps/overlap length	NCBI conserved domains/pfam	E-value	AlphaFold2/PDBeFOLD prediction	Signal Peptide	Trans-membrane helices	Suggested gene function	Essential for transfer ^d
<i>orf53587</i> (CAE92904.1)	505	VirB6 (WP.010974917.1)	11.9/ 482/641	TraG.N./07916	2.29e-71	No structural overlap ^c	–	5	Inner membrane protein	+
<i>orf55120</i> (CAE92905.1)	119	–	–	None	–	FrmR formaldehyde transcriptional repressor	–	3	Transcription regulator <i>pilT</i>	ND
<i>orf55476</i> (CAE92906.1)	465	VirB11 (WP.010974918.1)	3.7/ 695/752	Conjugal TIGR03755	0e + 00	No structural overlap	SPI	1	(<i>traU</i>)/ <i>iceU</i>	+
<i>orf56883</i> (CAE92907.1)	315	–	–	TraU superfamily	0e + 00	No structural overlap	SPI	–	–	+
<i>orf57827</i> (CAE92908.1)	148	–	–	DURF1525/pfam07511	2.07e-55	Thioredoxin-like protein	SPI	1	Disulfide oxidoreductase	+/-
<i>orf58432</i> (CAE92909.1)	164	–	–	PRK00024 super family	1.31e-62	DNA repair protein RadC	–	–	Putative DNA repair protein	–
<i>orf59110</i> (CAE92910.1)	254	–	–	DsbA family/Thioredoxin-like superfamily	5.78e-13	Protein disulfide isomerase	–	1	<i>dsbA</i>	–
<i>orf59888</i> (CAE92911.1)	955	VirB4 (WP.010974916.1)	29.4/ 362/1053	TraC.PFL.4706	0e00	Type VII Secretion ATPase EccC	–	–	Conjugative transfer ATPase (<i>virB4</i>)/ <i>iceB4</i>	+
<i>orf62755</i> (CAE92912.1)	146	–	–	conj_TIGR03751	5.9e-61	No structural overlap	SPII	–	Outer membrane protein	+
<i>orf63176</i> (CAE92913.1)	472	VirB10 (WP.010891494.1)	23.2/ 289/569	conj_TIGR03752	0e00	COMB10 of a COM-type IV secretion system	–	1	<i>virB10/iceB10</i>	+
<i>orf64584</i> (CAE92914.1)	310	VirB9 (WP.010891495.1)	29.1/ 145/374	TraK superfamily/pfam11920	1.67e-160	No structural overlap	SPI	1	<i>virB9/iceB9</i>	+
<i>orf65513</i> (CAE92915.1)	230	VirB8 (WP.010891496.1)	30.8/ 111/289	conj_TIGR03746	1.02e-127	Periplasmic domain of DotI/CagV	–	1	<i>virB8/iceB8</i>	+
<i>orf66202</i> (CAE92916.1)	136	VirB3 (WP.010891501.1)	7.5/ 184/213	DUF 3487/pfam11990	1.35e-48	No structural overlap	–	2	Inner membrane protein	+
<i>orf66625</i> (CAE92917.1)	119	VirB2 (WP.010891502.1)	25.9/76/158	conj_TIGR03745/DUF2976	4.69e-46	Conjugative pilus	SPI	3	Candidate major pilin/ <i>iceB2</i>	+
<i>orf67001</i> (CAE92918.1)	77	–	–	conj_TIGR03758/DUF3262	8.62e-21	Membrane anchor protein of succinate DH complex	–	2	Inner membrane protein	+
<i>orf67231</i> (CAE92919.1)	127	–	–	ICE_RAQPRD	7.35e-38	Modular repressor recruitment protein	SPI	–	Unknown	–
<i>orf67800</i> (CAE92920.1)	134	–	–	No match	–	No structural overlap	–	–	Unknown	–
<i>orf68241</i> (CAE92921.1)	249	–	–	conj_TIGR03747/DUF4400	3.54e-117	No structural overlap	–	4	Inner membrane protein	+
<i>orf68987</i> (CAE92922.1)	728	VirD4 (WP.065698658.1)	28.3/ 366/881	conj_TOL_TraD	0e+00	Coupling protein TrwB	–	2	<i>virD4/iceD4</i>	+
<i>orf71178</i> (CAE92923.1)	182	–	–	DUF 2859/ pfam11072	1.67e-72	Thiol-disulfide oxidoreductase	SPI	–	Thioredoxin-like	+/-
<i>orf71723</i> (CAE92924.1)	196	VirB1 (WP.010891503.1)	31.8/ 107/274	Lyz-like super family	2.51e-09	Lytic transglycosylase	SPI	–	<i>virB1/iceB1</i>	+/-
<i>orf72295</i> (CAE92925.1)	239	–	–	conj_TIGR03759	6.73e-112	Thiol-disulfide oxidoreductase	SPI	–	Thioredoxin-like	ND
<i>orf73029</i> (CAE92926.1)	216	–	–	No match	–	Membrane anchoring PilP protein.	–	–	Unknown	–
<i>orf73676</i> (CAE92927.1)	206	–	–	conj_PilL	9.91e-51	STN superfamily periplasmic signaling domain/DotD	SPII	–	<i>dotD/iceB7</i>	+

^aDesignation in GenBank AJ617740.2.^bArchetype Vir-T4SS of *A. tumefaciens*.^cOnly listed when RMSD > 3.^dsee Figure 2; ND, not determined.

Table 1). Two ATPases, IceB4 and IceD4, may associate on the cytoplasmic side of the inner membrane. A third ATPase and PilT analog, encoded by *orf55476*, may be located in the periplasm. An inner membrane complex (IMC) of the T4SS may be constituted by Orf53587, IceB8, Orf66202, Orf68241 and Orf67001 (Supplementary figure S2). In analogy, IceB10 would contact and span from the inner to the outer membrane complex (OMC), further com-

posed of IceB9 and IceB7, and possibly Orf62755. Finally, structural analysis suggested that the conjugative pilus might be formed from IceB2 (Orf66625) subunits (Supplementary figure S2). In absence of Vir-homolog, we renamed Orf56883 to IceU, following the Tra-nomenclature. A set of periplasmic proteins may complete or associate with the ICE-T4SS complex, including IceU, IceB1 and Orf67231, and the putative post-translational modifier proteins

Orf57827, Orf59110, Orf71178, Orf72295 and Orf73029 (Supplementary figure S2).

Gene deletions implicate ICE clc functions in conjugative transfer

To study their potential implication in ICE clc transfer, we individually deleted 22 out of the identified 24 open reading frames in the predicted T4SS-encoding region (Figure 1, Table 1). Deletions were created in-frame by leaving a stretch of 6–10 amino acids at the N- and C-terminal of the protein, to avoid polar effects. Neither single nor double deletions could be recovered of *orfs* *iceB2*, *67001* and *67231*, perhaps because of their small gene size. This was then replaced by a single deletion removing all the three consecutive genes (i.e. Δ *orf67231-iceB2*).

Deletions of 15 of the targeted genes caused a more than 100-fold decrease of ICE clc transfer rates in isogenic *P. putida* matings. These comprised both genes analogous to archetype T4SS components (i.e. *iceB4*, *iceB8*, *iceB9*, *iceB10*, *iceD4*, and *iceB7*, Figure 2A; see Figure 1B for original *orf* nomenclature and location, and Table 1), as well as those without clear T4SS counterparts (i.e. *orf53587*, *orf55476*, *iceU*, *orf62755*, *orf66202*, *orf67231-iceB2* and *orf68241*, Figure 2B). Two other deletions significantly affected ICE clc transfer, but less severely than the ones mentioned above. ICE transfer decreased by 50-fold in a Δ *iceB1* (*orf71723*) mutant (Figure 2A), and 10-fold in a Δ *orf71178* mutant compared to wild type (Figure 2B). Ectopic complementation with a single-copy wild-type gene under control of the ICE clc transfer competence P_{67231} -promoter restored transfer in all cases but one (i.e. *orf53587*, Figure 2A and B), indicating that deletion of *orf53587* might have caused a polar effect. However, for all the other deletions the transfer defect was attributable to the single gene knockout. Several deletions, e.g. of *orf55476*, *orf66202*, *orf67231-iceB2*, *orf71178*, *iceB7* or *iceB10*, were restored partly by ectopic complementation (Figure 2B). This might indicate that ectopic placement resulted in imbalanced expression levels or timing for functional complementation. Since the deletion of Δ *orf67231-iceB2* involved three consecutive genes, we further complemented this with each gene individually or in pairs, ectopically placed in single integrated copy under control of the P_{67231} -promoter (Supplementary figure S3). Only the combination of *orf67001-iceB2* partly restored transfer, suggesting they are the essential genes, whereas *orf67231* is not (Supplementary figure S3). In contrast, a further set of four gene deletions did not cause detectable effects on ICE transfer (*orf58432*, *orf59110*, *orf67800*, and *orf73029*, Figure 2C), whereas deletion of *orf57827* and its complementation reduced transfer by 4-fold (Figure 2C). This suggests them to have minor or no influence on ICE transfer, or to be functionally redundant.

We concluded from these results that the region in between *orf53587* and *orf73676* on ICE clc is indeed essential for its conjugation. The predicted ICE-T4SS is very dissimilar to archetypal plasmid T4SSs, except for a few distantly structurally related components (Supplementary figure S2). In contrast, the ICE-T4SS loci and gene synteny are highly conserved between ICE clc and genome regions in other β and γ -proteobacteria, suspected to carry similar ICEs (Fig-

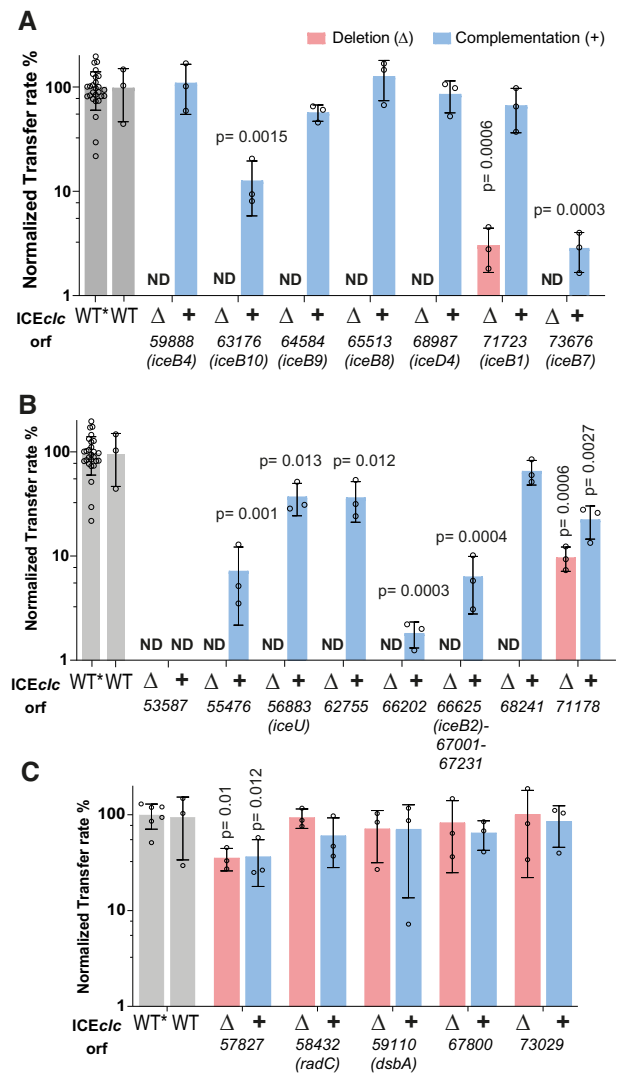


Figure 2. Effects of individual ICE clc gene deletion and complementation on transfer. (A) Deletion effects of ICE clc genes with distinct sequence and/or structural similarity to known T4SS components. (B) ICE clc genes without distinct sequence and structural similarity. (C) ICE clc genes with or without mild effect on transfer. Bars represent the mean normalized transfer rates of ICE with single gene deletions (Δ , salmon), or single copy complementations (+, blue), as percentage of that of wild-type ICE clc (grey) in *P. putida* UWC1 isogenic matings, each individually quantified as the frequency of transconjugant colony forming units (CFU) on selective medium per donor CFU. Error bars indicate calculated standard deviations on biological replicates, with small open circles showing the individual replicate values. *Orf* and gene names indicated below. ND, below detection limit ($<1\%$). WT, unmodified ICE clc wild-type. WT*, ICE clc carrying an integrated *lacO*-array; used for producing the deletions and complementations. Note that the same WT and WT* rates are reproduced in all panels for ease of comparison. *P*-values were calculated with a two-tailed *t*-test between wild-type (WT*) and mutant replicate rates (as percentages). Only *P*-values <0.05 are shown.

ure 3). This strongly suggests functional conservation, even for those genes whose deletion on ICE clc did not directly affect isogenic transfer rates. Two sites (nearby *orf67800* and *orf58432* on ICE clc) were permissive for gene loss in the other compared genomic regions (Figure 3). Nevertheless, the strong conservation of gene order and overall similar-

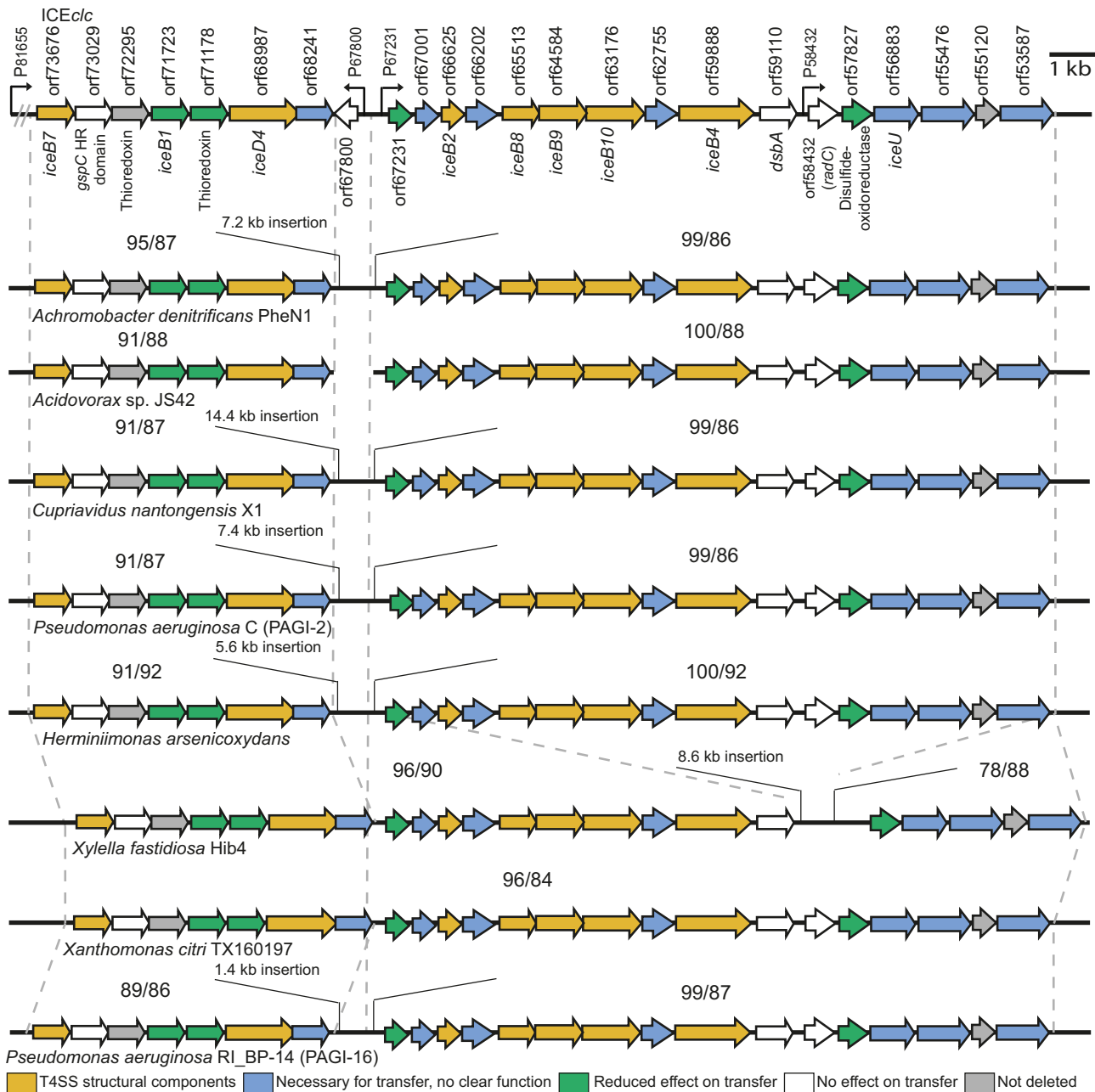


Figure 3. ICE clc transfer region gene and synteny conservation. Genetic organization of the ICE clc conjugative system gene loci (top), aligned with corresponding regions within the genomes of eight other β - and γ -Proteobacteria. The dotted lines delimit the regions of synteny to ICE clc , with numbers representing the sequence coverage (left) and the percentage of nucleotide identity (right), respectively. Arrows indicate coding frames and their orientations, with filled colors representing transfer effects as in the legend on the bottom of the figure.

ity is an indication that these are parts of mobile elements capable of producing T4SS conjugative systems for which ICE clc is a representative model.

Subcellular localization of the ICE clc conjugative system proteins

To further corroborate bioinformatic predictions and transfer results, we investigated the subcellular localization of nine of the encoded proteins in the ICE clc conjugative system gene region. This choice was not exhaustive, but

contained a number of predicted structurally ‘known’ (e.g. IceB4, IceB7, IceB8) as well as less clear components (e.g. Orf66202, Orf55476, outlined in Figure 1C), and targeting both proteins predicted to be associated to the inner and outer membranes, as well as those with predicted periplasmic localization. In order to visualize protein localization, we translationally fused the target open reading frames within their original ICE clc locus with the reading frame of super-folder green fluorescent protein (*sfGFP*) or of *mCherry*, separated by a small linker peptide to avoid folding complications, as in Ref. (32). This approach was expected to

best preserve stoichiometry and timing of fusion protein production with respect to the native ICE*clc* counterpart. Our hypothesis here was that if the targeted protein would be part of a multi-component and multi-subunit T4SS complex, expressing the fluorescent protein fusion might result in a well-defined fluorescent spot, whereas if it would not be part of the T4SS, its fluorescence would be homogeneously distributed in the cytoplasm or in the cell envelope. We chose a combination of both sfGFP and mCherry in order to test for colocalization of different components (see below). To test for functionality of the expressed fluorescent fusion protein, we quantified ICE transfer from respective *P. putida* donors and compared this to wild-type ICE. We assumed similar transfer rates to be the best indication for proper functionality, in which case we concluded that the position and/or distribution of the observed fluorescence was representative for the true (non-labeled) protein localization.

All tested ICE-fusion proteins produced multiple clear fluorescent foci in stationary phase *P. putida* cells, with in about half of the cases, accentuated fluorescent cell outlines (Figure 4A). As expected from previous studies using transcriptional fusions to key ICE*clc* transfer competence promoters (7,21), fluorescent fusion protein expression was limited to a subpopulation of cells appearing in stationary phase (Figure 4B). These subpopulations reached similar abundances for the different constructs, as deduced from quantile-quantile plots of observed versus expected normal distribution of fluorescence values (Figure 4B, light brown-shaded regions). A co-expressed cytoplasmic marker for transfer competence (P_{inR} -*echerry*) labeled the same cells as those displaying the fluorescent fusion protein-signal in stationary phase (Supplementary Figure S4A). This would be in agreement with the hypothesis that only tc cells assemble the ICE conjugative machinery. Foci were situated near the cell edge in high-resolution images (Figure 4A, Airyscan), coinciding with stained cell membranes (Supplementary Figure S4B), as expected for a membrane-spanning protein complex such as the T4SS. Because of the limited throughput in high-resolution microscopy (i.e. Figure 4A, Airyscan) we quantified foci numbers from larger numbers of cells (1000–10 000 per replicate per strain) imaged in regular epifluorescence microscopy, and using a threshold for foci detection based on differences in foci scores among non-tc and tc cells (Figure 4B). This confirmed the high-resolution visual aspects; notably, the occurrence of multiple foci per cell in case of fusions to IceD4, IceB4, IceB7, iceB8, Orf55476 and Orf66202 (Figure 4C). In contrast, fusions to IceU, Orf62755 and Orf71178 showed fewer quantifiable foci, also in agreement with the high resolution aspect of the cell envelope outlines (Figure 4C, Supplementary Figure S5).

ICE transfer rates from *P. putida* donors were unaffected for seven of the nine tested fluorescent protein fusions, suggesting no functional impairments (Figure 4D). In contrast, donors expressing sfGFP-IceB8 or mCherry-Orf62755 reduced ICE transfer by 10- and 50-fold, respectively, compared to wild-type, indicating loss of some aspect of functionality by the fluorescent protein fusion (Figure 4D).

To provide further evidence that the observed fluorescent foci were specific for conjugation complexes in *P. putida* ICE*clc* tc cells, and not the result of aberrant or sponta-

neous fluorescent protein aggregation, we studied control strains of *P. putida* ICE*clc* expressing only sfGFP from the same P_{67231} promoter but artificially induced in all cells by overexpression of the ICE-transcription factor BisR (7). These cells showed no detectable foci but homogenous cytoplasmic fluorescence, indicating that sfGFP does not self-aggregate into fluorescent foci at the cell envelope (Figure 4E and Supplementary figure S4C). Secondly, we expressed the *iceB4-sfgfp* or *iceD4-sfgfp* fusions in all cells of *P. putida* UWC1 devoid of ICE*clc*, through induction with the ICE-transcription factor complex BisDC (7). These cell populations showed very little fluorescence, with some 0.2% outliers from quantile-plotting (Figure 4E). Sporadic low-intensity foci were observed among this subpopulation of fluorescent cells (Figure 4E, Supplementary figure S4D and E), appearing at polar regions and accompanied by cellular morphological aberrations (Figure 4E). Although there is a tendency of expressed IceB4- or IceD4-sfGFP protein to aggregate into sporadic fluorescent foci, this frequency is 10- to 50-fold lower than appearing clear foci in envelopes of *P. putida* tc cells carrying ICE*clc*. It is therefore very unlikely that the multiple bright foci detected with six of the fluorescently tagged ICE conjugative proteins (Figure 4C) consist of autoaggregated misfolded proteins.

Colocalization of dual-labeled ICE*clc* conjugative system components

In order to determine whether the multiple foci seen in tc cells for different fluorescently-tagged ICE proteins were likely part of the same macromolecular protein complexes, we quantified the colocalization of sfGFP and mCherry signals in *P. putida* ICE*clc* hosts expressing double-labeled components. We chose for this a combination of either *iceB4-sfgfp* and *iceB7-mcherry*, or *iceB4-sfgfp* and *orf55476-mCherry*. ICE transfer rates from donors with the double label IceB4-IceB7 combination was again very close to wild-type transfer rates (Figure 5A), suggesting retained functionality. Double labeling of IceB4 and Orf55476 resulted in a tenfold decrease in mean transfer rate compared to wild-type – although this was not statistically significant (Figure 5A).

We assumed foci overlap at geometric distances within 165 nm (2.5 pixels on the images), and imaged potential colocalization in deconvoluted high-resolution 170-nm cell slices. Visual inspection from high-resolution images of *P. putida* expressing double fusions confirmed that the two proteins are expressed simultaneously in tc cells and suggested mostly overlapping foci, but not exclusively (Figure 5B, C). Quantification of foci distances on larger numbers of tc cells from epifluorescence images, indicated that on average between 1 and 4 foci overlapped in 70% of tc cells with dual IceB4- and IceB7-labeling, and 83% of tc cells in case of strains with both IceB4-sfGFP and Orf55476-mCherry labeling (Figure 5D).

In conclusion, the microscopy and transfer experiments indicated that fluorescent foci observed in stationary phase tc cells of *P. putida* ICE*clc* are most likely representative for the formation and positions of multimeric protein complexes such as expected from the T4SS, and not the result of spontaneous aggregation of the fluorescent protein

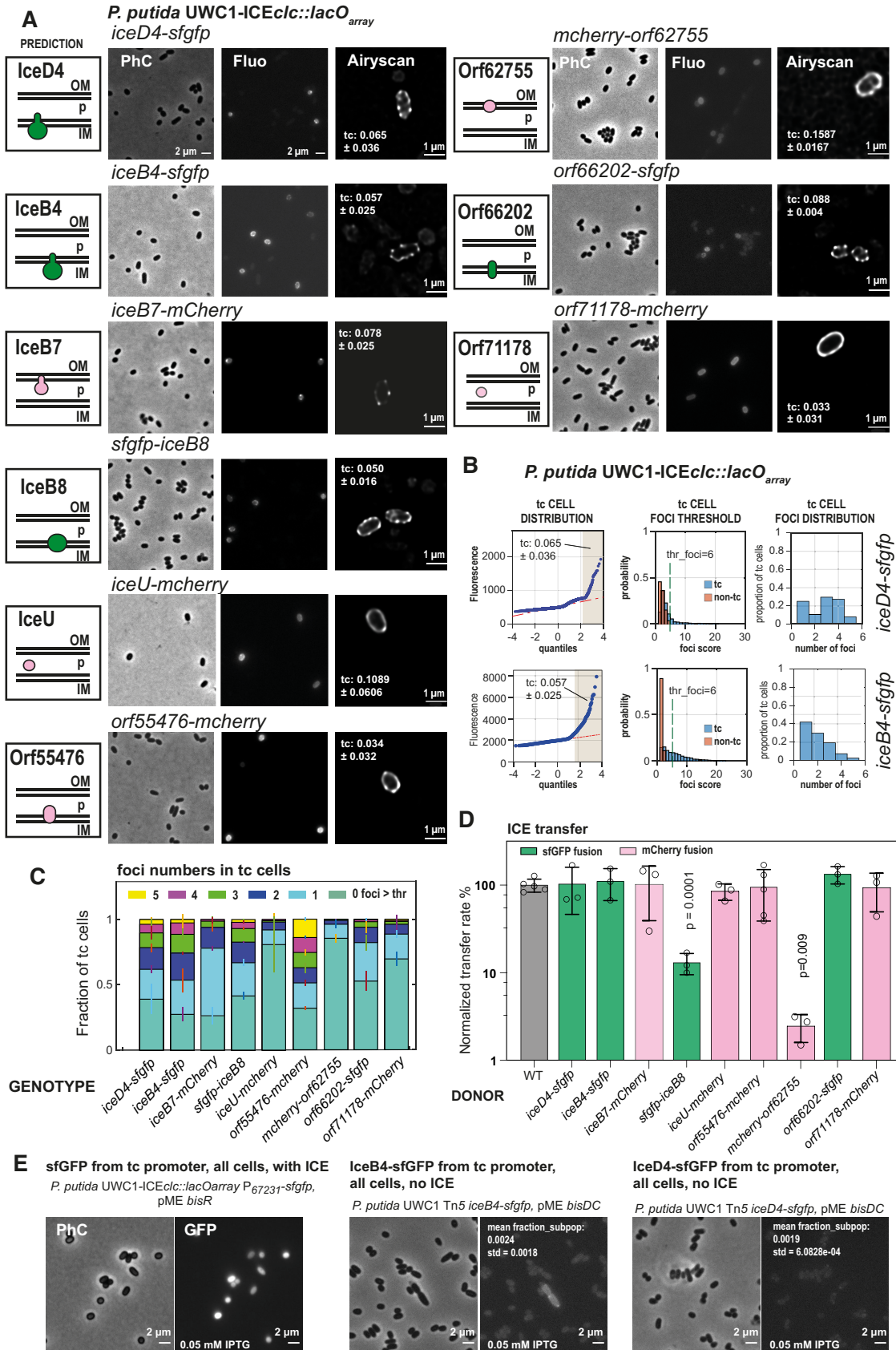


Figure 4. Subcellular localization of predicted ICE*clc* conjugative system subcomponents. (A) Micrographs of *P. putida* strains with indicated fluorescent-protein-tagged conjugative system components, imaged in stationary phase cultures after growth on 3-CBA. Panels on the left show the bioinformatic

fusions. Obtaining similar foci-per-cell numbers in case of fusions to IceD4, IceB4, IceB7, IceB8 (despite its partial loss of functionality), Orf55476 and Orf66202 is very suggestive for these proteins to be part of the same multiprotein complexes, which was confirmed to some extent by the fluorescent marker overlap in double-labeled strains. The different fluorescence aspect (e.g. stronger cell envelope outlines) of the IceU- and Orf71178- fusions (the Orf62755-fusion being impaired for ICE transfer) may be an indication for them not being integral part of a T4SS and performing a different role in the ICE conjugative process.

Interdependencies among subcomponents of the ICE*clc* conjugative system

Finally, we studied potential dependencies of the observed foci formation on other predicted components of the ICE conjugative system. The same fluorescent protein fusion constructions were reproduced in their native locus in *P. putida* that further carried single copy deletions in ICE*clc* conjugative system genes, and effects of the deletions on fluorescent signals were examined (Figure 6A–C). Apart from direct high-resolution cell images we focused on three aspects of fluorescence measurements that we expected to yield quantifiable differences. First of all, we assumed that observed foci intensities might diminish, for example, if fewer of the tagged protein subunits would assemble into the T4SS structure, or if their turnover would be faster in absence of proper assembly. Secondly, we expected that mutations might lead to fewer fluorescent foci per cell, for example, as a result of T4SS assembly failures. This might then result in enrichment of the fluorescence signal of the tagged protein in, for example, the cell envelope. Finally, we imagined that quantifiable differences in foci ‘aspects’ might occur in mutants (i.e. blurring; visible from fitting scores and Gaussian sigma values, Supplementary Figure S1D and E), due to impaired T4SS assembly or misfolded multimeric structures. We quantified these parameters from epifluorescence imaging of tc cell subpopulations (142–1996 tc cells per replicate) in stationary phase cultures and in comparison to wild-type tagged constructs in biological independent triplicates to calculate statistical significance. We do acknowledge that at the resolution of EFM and the Airyscan, observed differences may have different underlying causes from what we assumed.

As an example, in case of IceB4-sfGFP background (Figure 6A), all tested deletions except that of *orf68241*, affected some aspect of fluorescent foci formation (Supplementary table S4). This was mostly quantifiable as generally weaker and more diffuse foci (Figure 6B, C, Supplementary Figure S6), and more cells without any detectable foci (Figure 6D). There was no increase in the median tc-cell cytoplasmic fluorescence intensity as a result of lowered foci intensities in mutants (Supplementary Table S5), but the estimated sizes of the tc population remained the same (Supplementary Table S5). Altogether, this would indicate that IceB4-sfGFP assembly into fluorescent foci is directly or indirectly dependent on IceB7, IceB8, Orf66202, Orf53587 and IceB10, but not on Orf68241. All of these deletions by themselves completely abolish ICE transfer (Figure 2), and, therefore, loss of IceB4-sfGFP foci formation would be in agreement with an impairment of proper multi-component T4SS assembly.

A number of other deletions were tested in the IceB7-mCherry, sfGFP-IceB8, IceD4-sfGFP and Orf55476-mCherry backgrounds, the effects of which are summarized in Figure 7. Deletions of either *iceB9* or *orf62755* in IceB7-mCherry background resulted in weaker and fewer foci in tc cells, whereas effects of an *iceB10* deletion were inconclusive (Figure 6C and D, Supplementary Figure S7). Similar as in case of IceB4-sfGFP background, the deletion of *orf68241* did not measurably change foci numbers of sfGFP-IceB8, whereas deletion of *orf53587* caused foci to become weaker and more blurred (Figure 6C and D, Figure 7, Supplementary Figure S8). Both deletions of *iceB4* or *iceB10* yielded weaker and fewer IceD4-sfGFP foci (Figure 6C and D, Figure 7, Supplementary Figure S9). Finally, deletion of *iceB4* in Orf55476-mCherry background produced more foci variability, whereas deletion of *orf68241* resulted in weaker foci and clearer cell outlines (Supplementary Figure S10). Since all the deletions individually by themselves abolish ICE*clc* transfer, these different aspects of foci fluorescence in mutant strains (Figure 7) suggest impairments and/or losses of proper assembly of the multimeric multiprotein conjugative complexes, as will be discussed further below.

DISCUSSION

We performed a systematic analysis of the gene functions involved in ICE*clc* conjugation as representative of the

prediction of the protein’s localization with respect to inner membrane (IM), periplasmic space (P) or outer membrane (OM); green, sfGFP-tagged protein fusion; magenta, mCherry-fusion. PhC, Phase contrast; Flu, fluorescent channel. Airyscan, high-resolution deconvoluted 170-nm image slice of the respective strain. Proportion of observed tc cells (mean \pm one SD of individual biological triplicates) indicated within the Airyscan panels. (B) Example of tc cell foci quantification on epifluorescence images of *P. putida* ICE*clc* hosts expressing either IceB4- or IceD4-sfGFP; quantile-quantile plot of median fluorescence per cell measured on a single replicate set of images for the different strains and showing the derived tc cell subpopulation (highlighted in light brown and its mean proportion \pm one SD). Thresholds (thr.foci) used for distinguishing foci for the relevant indicated labeled constructs in tc cells (blue bars) from spurious background ‘foci’ in the majority of non-tc cells (red bars), based on calculated foci intensities from Gaussian fitting. Plots show probability normalized distributions of foci intensities among the two cell groups (differentiated based on quantile-quantile plots). Derived number of foci per cell at the indicated threshold (thr.foci) for a single replicate. (C) Stack plots showing the mean proportions of foci (\pm one SD from biological triplicates) above threshold in tc cells for all constructs shown in panel (A). (D) Wild-type normalized mean ICE*clc* transfer rates (\pm one SD from biological triplicates; circles showing individual data points) from the fluorescent protein tagged donor strains into *P. putida* recipients. Differences compared to wild-type were assessed with a two-tailed t-test on biological triplicate pairs (if not indicated, p-values were >0.1). (E) Micrographs of control strains *P. putida* UWC1 ICE*clc-lacO*_{array} expressing sfGFP from the P₆₇₂₃₁-promoter, and of *P. putida* UWC1 devoid of ICE*clc* expressing IceB4-sfGFP or IceD4-sfGFP. P₆₇₂₃₁-promoter activation was induced in all cells by overexpressing the proteins BisR or BisDC in presence of 0.05 mM IPTG, two known regulators of ICE*clc* activation cascade (7). Numbers indicate the mean proportion of the subpopulation of cells in quantile-quantile plots from biological triplicates (± 1 SD).

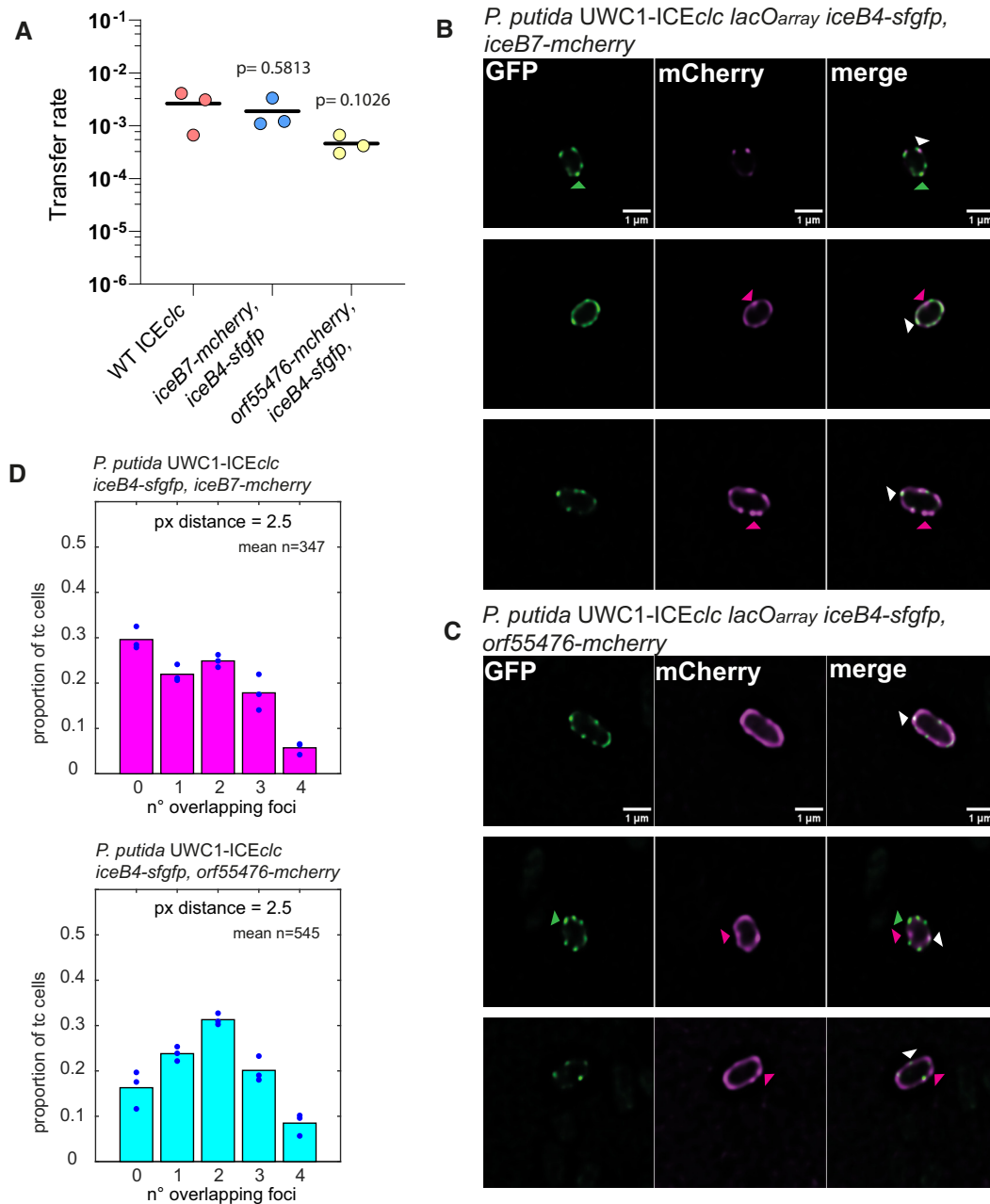


Figure 5. Colocalization of dual-labeled components of the ICEclc conjugative system in *P. putida*. (A) Mean transfer rates (lines, as frequency of transjugant CFU on selective medium per donor CFU) of ICEclc in isogenic *P. putida* matings from wild-type donors or ICE with dual-labeled fluorescent protein constructs, as indicated. Dots depict individual replicate transfer rates with p-values showing the probability of means being dissimilar in two-tailed *t*-test comparisons. (B and C) Micrographs of individual tc cells of *P. putida* ICEclc::lacOarray, expressing both IceB4-sfGFP and IceB7-mCherry, or IceB4-sfGFP and Orf55476-mCherry, imaged in stationary phase after growth on 3-CBA in their proper individual fluorescent channel (sfGFP, mCherry), or presented as overlay (merge, GFP is green; mCherry is magenta). Images composed of a single 170-nm deconvoluted slice in Airyscan microscopy. Colored triangles in (B) and (C) point to examples of non-colocalized (green or magenta) or overlapping foci (white). (D) Measured mean proportions (bars) of the number of overlapping GFP and mCherry foci (between 1 and 4) in tc cells of both strains (overlap is within a minimum distance of 2.5 pixel or 165 nm of the fitted 2D-Gaussian foci centres). Circles are individual replicate values. n = mean number of tc cells per replicate.

poorly studied MPF_G clade of T4SS conjugation systems (14). Our results indicate that ICEclc encodes a conjugative system that has both a number of structurally analogous components to known T4SS, as well as several crucial unique and unknown components (Table 1). The unique components are common to a wide class of elements related to ICEclc. We further find that formation of the ICEclc-

T4SS is restricted to transfer competent (tc) cells, which can carry multiple such systems per cell as judged from microscope imaging. The occurrence of multiple T4SS per *P. putida* ICEclc tc cell is similar as what was found for labeled Vir-components in case of *Agrobacterium tumefaciens* (25,46) and from cryo-tomography of *Legionella pneumophila* Dot/Icm cells (27), and may contribute to

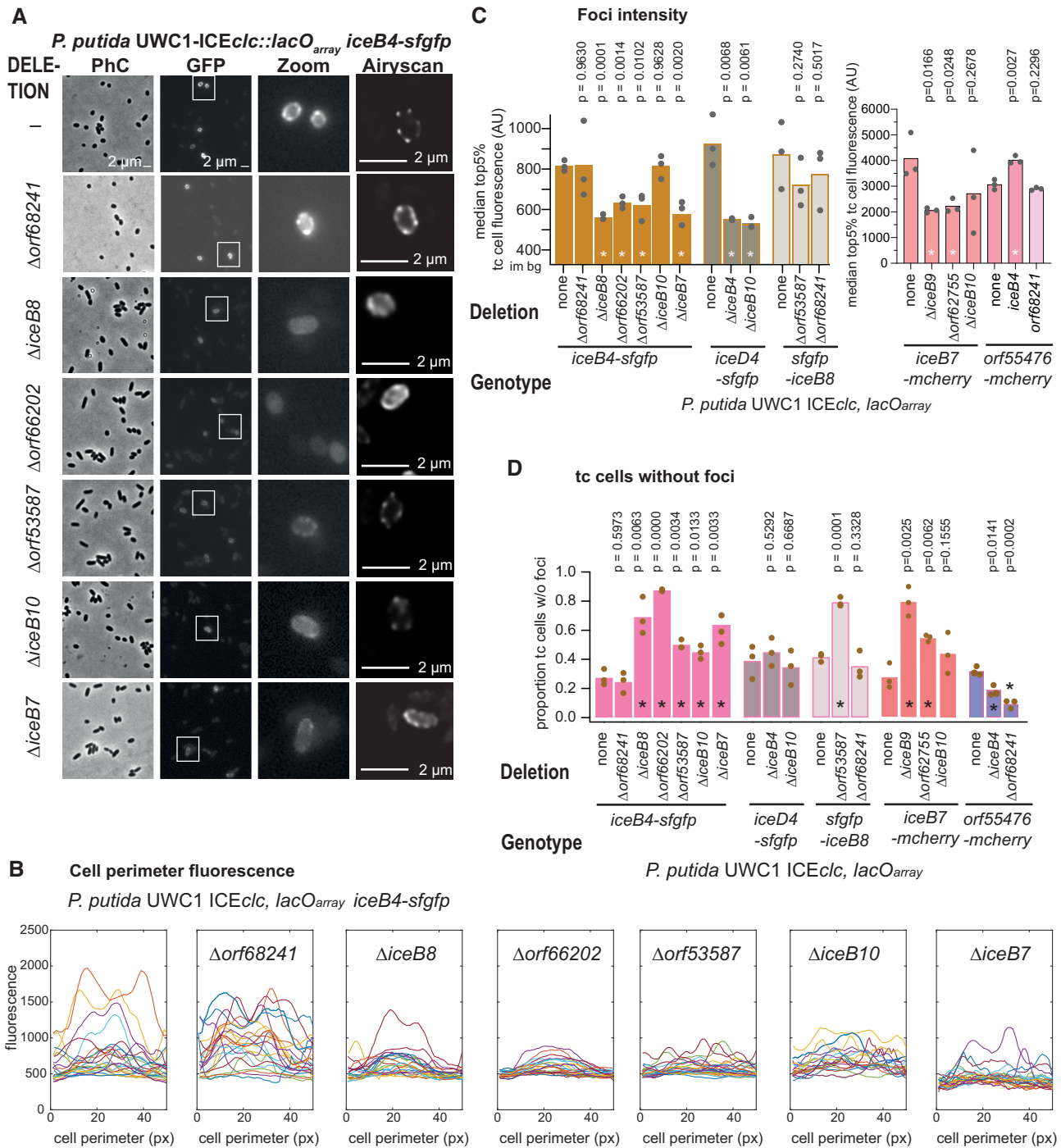


Figure 6. Dependencies among subcomponents of the ICE*clc* conjugative system. **(A)** Visible aspect of IceB4-sfGFP foci formation in *P. putida* in stationary phase after growth on 3-CBA with a single integrated copy of (otherwise) wild-type ICE*clc*::lacO_{array}, in comparison to additional deletions of *orf68241*, *iceB8*, *orf66202*, *orf53587*, *iceB10*, or *iceB7*. Micrographs as in Figure 4 with a highlighted cell area (Zoom) from the GFP image and a high-resolution Airyscan image (single 170-nm slice). Images are scaled to the same maximum and minimum intensities. **(B)** sfGFP fluorescence traces of the perimeter of individual tc cells (1-pixel outer ‘shell’) of the indicated constructs in panel (A) on their absolute fluorescent scales. ‘Peaks’ correspond to foci in the cell micrographs. **(C)** Mean top 5% median fluorescence among tc cells (bars, indicative for foci intensity) among biological triplicates of the different labeled strains in wild-type or mutant backgrounds (circles showing individual replicate values; im bg, image background fluorescence). P-values result from paired two-tailed t-test comparisons of mutant to wild-type (asterisks indicating significance at 0.05 or below). **(D)** As C, but for the mean proportion of tc cells without detectable foci (threshold determination as in Figure 4). All other individual strain micrographs and foci analysis are presented in Supplementary figures (see main text).

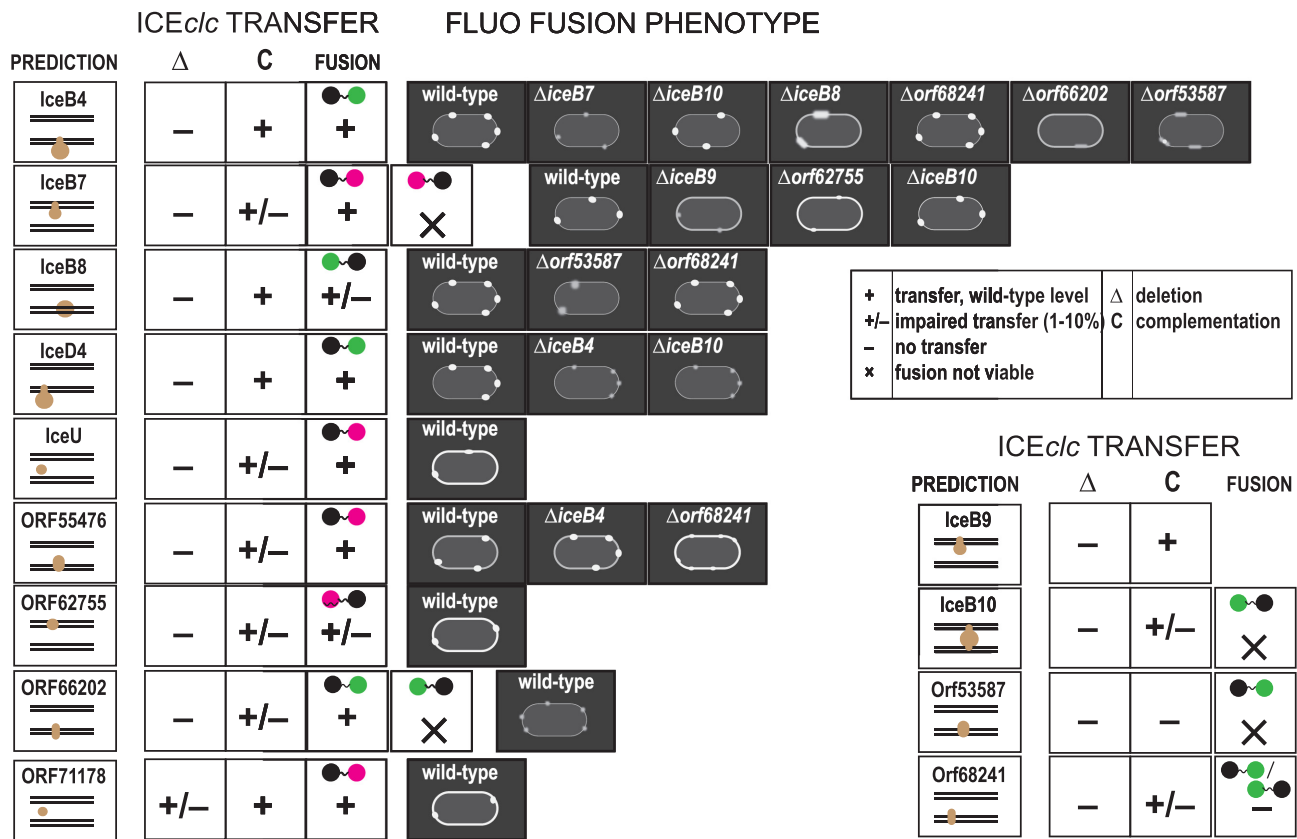


Figure 7. Schematic summary presentation of subcomponent dependencies in the ICE*clc* conjugative system, derived from transfer, mutant and fluorescent protein fusion studies. Panels show for each of the tested component the bioinformatic prediction of its localization, the ICE*clc* transfer frequency of its deletion mutant (Δ) and the complementation (C), and of the fusion construct (magenta, mCherry fusion; green, sfGFP; black circle, targeted protein). Fluorescent protein fusion phenotypes schematically indicated for the type (crisp, small, fuzzy) and numbers of foci observed, and cell envelope fluorescence characteristic (thick, more pronounced outline). Qualitative indication of transfer rates as in the legend, corresponding to measured values as in Figure 4D.

the efficiency of the ICE to transfer from specialized cells (11,47).

Despite representing its rightful separate evolutionary lineage, the T4SS of ICE*clc* has parallel structural and functional analogies to other widespread types such as Mpf_T and Mpf_F. Our functionality analysis was based on detailed bioinformatic structural analysis, individual gene deletion and complementation studies, fluorescent fusion protein analysis, and their effects on ICE transfer. Mating-pair formation complexes can comprise between 12 and more than 20 individual proteins (48,49). We found 14–15 essential elements within the ICE*clc* conjugative gene region (including *traI*, Figure 1). Weak full length amino acid similarities and predicted structural homologies enabled to classify analogs of archetypal T4SS structural components within the ICE*clc* system, which we named IceB2 (for VirB2 analog, etc.), IceB4, IceB7, IceB8, IceB9, IceB10, and IceD4, as well as unknown components (e.g. Orf55476, Orf53587; Table 1). Indeed, their deletion abolished ICE*clc* transfer, whereas ectopic single copy complementation under control of a transfer competence promoter partly or fully restored it, indicating clear gene-dependent effects. Microscopy imaging of strains expressing translational fluorescent protein fusions from their native ICE*clc* loci showed that IceD4, IceB4, IceB8, and IceB7 fusions form clearly

localized fluorescent foci in the cell envelope. Of these, IceD4-, IceB4- and IceB7-fusions retained wild-type transfer rates, confirming their functionality. Mutation studies in backgrounds of fluorescently-tagged ICE proteins, indicated that foci formation of IceB4-sfGFP was impaired by additional deletions of *iceB7*, *iceB8*, *iceB10*, *orf53587* and *orf66202*; of IceD4-sfGFP by deletions of *iceB4* and *iceB10*, and of IceB7-mCherry by *iceB9* or *orf62755* (Figure 7). Since these deletions in wild-type background completely abolish ICE-transfer, this strongly suggests that foci consist of the ICE-T4SS conjugation machines, which cannot correctly assembly in absence of their core components. This is consistent with a hypothesis of IceB4, IceB7, IceB8, IceB9, IceB10 and IceD4 being part of a multicomponent structure similar to known plasmid-type T4SSs (schematically assigned as in Supplementary figure S2A).

Various analogies can be drawn from other T4SSs and our results on the ICE*clc* system, which support the hypothesis of their overall structural resemblance. For example, the localization of IceB4 (the predicted cytoplasmic ATPase) to the ICE*clc*-T4SS required the presence of Orf66202, IceB8, Orf53587, IceB10 and IceB7 proteins (predicted inner and outer membrane components). This would be in agreement with observed dependencies of the VirB4-analog DotO protein of the Dot/Icm T4SS in *L. pneumophila* (50), and

crucial documented protein-protein interactions between VirB4 and either VirB3 or VirB8, and between VirB3 and VirB8 (51–53). Fluorescent protein fusions to Orf66202 also formed multiple visible foci (albeit weaker than to IceB4) in the cell envelope of tc cells (Figure 7), and remained functionally intact. Orf66202 is a predicted inner membrane protein with two transmembrane helices, and, in that sense, may have a similar role as VirB3 (54), although there was no detectable sequence or structural similarity between Orf66202 and VirB3. Although we did not manage to obtain a viable fluorescent protein fusion to Orf53587 (Figure 7), deletion of its gene disturbed formation of both IceB4-sfGFP and sfGFP-IceB8 foci, suggesting it is involved in T4SS assembly. Orf53587 is also predicted to be an inner membrane protein, with five trans-membrane helices, which is analogous to the *A. tumefaciens* VirB6 protein (55). Therefore, Orf53587 of ICE*clc* may have a similar role. VirB6 and VirB8 dependencies have also been described (56), which would then be in agreement with the effects observed here for the *orf53587* deletion on sfGFP-IceB8 foci. We acknowledge that sfGFP-IceB8 labeling caused a ten-fold decrease of ICE transfer, indicative for partial functionality, but its foci were crisp and strongly similar in numbers to those of completely functional fusions, e.g. IceB4-sfGFP. We assume, therefore, that sfGFP-IceB8 foci are still representative for the ICE*clc* conjugative systems localization in the cell, which in absence of Orf53587 cannot assemble properly (Figure 7).

As far as tested here, IceD4 association to the conjugative systems seemed to be dependent on IceB4 and IceB10, which we concluded from strongly diminished IceD4-sfGFP foci intensity and foci numbers in their absence (Figure 7). IceD4 is the predicted analog of the coupling protein ATPase, which is thought to oligomerize and activate only upon substrate binding (57). IceD4, with its two predicted trans-membrane (TM) helices in the N-terminal region, probably has natural affinity for the cytoplasmic membrane. Weaker IceD4-sfGFP foci intensities in absence of *iceB4* may thus be the consequence of IceD4 missing its molecular interaction partner, leading to destabilization of protein contacts, even though the T4SS core complex itself would be present. Cryo-EM studies on the R388 plasmid system showed that its VirD4 coupling protein indeed locates in close proximity of VirB4 (58). In case of *iceB10* deletion, the IceD4-sfGFP foci are hardly distinguishable from spurious background (Supplementary figure S9). Unfortunately, IceB10 fluorescent protein fusions were not viable (Figure 7), and the reciprocal localization experiment could not be tested. Therefore, we have to assume that in absence of IceB10, with its predicted core structural role, the ICE conjugative system is not properly assembled; leaving IceD4 without interaction partners. This idea is supported by previous studies of the *A. tumefaciens* T4SS, demonstrating conformational changes in VirB10 upon ATP hydrolysis by VirD4 (59).

We further found that IceB7-mCherry foci formation depended on IceB9 (Figure 7), analogs of which are known to form together the outer membrane channel part of the T4SS (43), which suggests similar protein contacts for the ICE*clc*-system. The dependency of IceB7-mCherry foci for-

mation on Orf62755 has not been previously documented. Orf62755 is a predicted outer membrane protein but without other known structural homology, and its membrane localization was illustrated by the patchy cell envelope fluorescence observed in an mCherry-fusion Orf62755-labeled strain (Figure 7). However, this fusion strain was only partly functional in ICE-transfer, and the localization of its fluorescence may not be completely informative. Orf62755 deletion strongly reduced foci formation of IceB7-mCherry, which would indicate that it is involved in T4SS assembly or a structural component of it.

Finally, one other ICE*clc* essential transfer protein (Orf55476), may be a further structural part of its T4SS. Orf55476-mCherry fusions were functional in ICE transfer and largely colocalized with IceB4-sfGFP foci in individual cells, but formed without strong dependence on *iceB4* (Figure 7). Orf55476 is a distant relative of a proposed PilT-analog in the ICE*Hin1056* element (15), which are more broadly known as ATPases that energize retraction of the Type IV pilus used for twitching motility and natural transformation (60). We hypothesize, therefore, that Orf55476 is an ICE*clc* T4SS-associated protein; possibly implicated in its pilus dynamics. Interestingly, Orf55476-mCherry foci formation was dependent on the presence of Orf68241, itself a transfer-essential protein, but for which neither N- nor C-terminal sfGFP-fused protein was functionally active (Figure 7). As mentioned, deletion of *orf68241* did not influence IceB4-sfGFP foci formation nor that of sfGFP-IceB8 (Figure 7). These results may thus indicate a specific and transient structural linkage between Orf68241 and Orf55476.

Apart from the structural T4SS analog proteins mentioned above, our analysis included predicted proteins without any sequence homology nor structural similarities to other functionally characterized proteins. One of these (IceU, product of *orf56883*) has an analog in TraU. The function of TraU remains unclear, although its absence was shown to reduce pilus formation and decrease transfer rates of the F-plasmid in *E. coli* (44). Our fluorescent reporter fusion to IceU was transfer-functional and localized to the cell envelope, producing occasional foci, in agreement with its predicted periplasmic situation (Figure 7). This suggests its role in transfer to reside in some transient interaction with T4SS complexes.

Deletions of other individual genes in the ICE*clc* T4SS gene region partly inhibited conjugative transfer or were without any noticeable effect altogether. Some of these have clear predicted functions, such as *iceB1* (*orf71723*, lytic transglycosylase), *orf58432* (RadC family), or *orf59110* (thiol disulphide oxidoreductase, DsbA). Lytic transglycosylases are frequently present in T4SS conjugative systems (61). Their assumed role is to locally degrade peptidoglycan and facilitate T4SS complex formation. Despite this, they are not essential for conjugation (62). Indeed, *iceB1* deletion reduced ICE transfer to ~3% compared to the wild type, which is similar to what was observed for deletion of the functional analog VirB1 in the *A. tumefaciens* system (62). Four genes in the ICE*clc* T4SS locus are predicted to encode thioredoxin homologs (Table 1). Similar numbers of thioredoxins have also been documented for other T4SS, such as from the F- and R27-plasmids of *E. coli* (63). These

proteins are supposed to facilitate folding or stabilization of the periplasmic, pilin and outer membrane subunits of the T4SS. Their mild (10-fold reduction, for *orf71178*; and 4-fold, for *orf57827*) to no influence on ICE*clc* transfer upon individual deletion can be explained by functional redundancies. The Orf71178-mCherry fusion was functional and localized in the cell envelope with diffuse foci (Figure 4 and 7, and Supplementary figure S5), which might be congruent with a presumed chaperone-like role. Attempts to delete *orf72295* on ICE*clc* were not successful; therefore, it may have some other essential role. Finally, the presence of a well-conserved *radC*-homolog (*orf58432*) on ICE*clc* and its family members remains enigmatic. These widespread proteins were initially thought to have a role in DNA repair at the replication fork (64), and some *radC* are expressed during the competence state in naturally transformable bacteria (65–67). In spite of that, inactivation of *radC* did not influence the efficiency of DNA uptake (68,69) and also deletion of *orf58432* on ICE*clc* had no measurable effect on conjugation rates.

The combination of mutation analysis and foci quantification gives a relatively coherent picture on the ICE*clc* conjugative system, but, evidently, the analysis of fluorescent foci in tc cells comes with uncertainty from limited resolution. Controls in isogenic *P. putida* without ICE*clc* but with overexpressed fluorescent proteins in all cells clearly indicate that the tc cell foci are not the result of unspecific fluorescent protein aggregation, but must be reflections of T4SS subunit multimerization. Furthermore, the combination of higher resolution Airyscan deconvoluted imaging of 170-nm cell slices with epifluorescence foci imaging across large numbers of tc cells provided quantifiable foci features with statistically sound comparisons among the various tagged protein constructs and additional ICE*clc*-gene deletions. Finally, there is precedent for observation of multiple fluorescent foci per cell from tagged T4SS proteins in *A. tumefaciens* (46), which suggested multiple T4SS units to be formed per cell. This was recently confirmed by cryo-tomography of the Dot/Icm system of *L. pneumophila* showing multiple T4SS complexes in individual cells (27). However, complexes seen in high-resolution microscopy by fluorescence tagging may not be consisting of the same T4SS assembly states, as demonstrated by recent cryo-EM studies of *E. coli* F-plasmid T4SS complexes in mini-cells, which revealed four distinct structural configurations (24).

In conclusion, we provide a detailed characterization of the ICE*clc* conjugative system and its subcellular localization, which is congruent to known plasmid-type T4SSs, but with a number of distinct and unknown structural elements as well as hitherto unreported dependencies. The ICE*clc* gene loci in this region are highly conserved in other Beta- and Gammaproteobacteria, both in sequence and gene synteny. The high conservation of T4SS gene regions in a variety of hosts is supportive for the hypothesis that they are part of other ICE*clc*-family elements, as proposed previously (7,17). Some of those, particularly in *P. aeruginosa* isolates, carry antibiotic resistance cassettes (70,71), suggesting that they encode active conjugative systems and are being selected for their efficient transfer. It is thus important to further unravel the details and potential dynamic steps in T4SS assembly and gene transfer.

DATA AVAILABILITY

The data underlying this article are available in the article and in its online supplementary material.

SUPPLEMENTARY DATA

Supplementary Data are available at NAR Online.

ACKNOWLEDGEMENTS

The authors thank Nicolas Carraro and Stephan Gruber for critical reading of the manuscript, and Justine Collier for advice.

FUNDING

Swiss National Science Foundation [31003A_175638, 310030_204897]. Funding for open access charge: Swiss National Science Foundation.

Conflict of interest statement. None declared.

REFERENCES

- Johnson, C.M. and Grossman, A.D. (2015) Integrative and conjugative elements (ICEs): what they do and how they work. *Annu. Rev. Genet.*, **49**, 577–601.
- Juhas, M., van der Meer, J.R., Gaillard, M., Harding, R.M., Hood, D.W. and Crook, D.W. (2009) Genomic islands: tools of bacterial horizontal gene transfer and evolution. *FEMS Microbiol. Rev.*, **33**, 376–393.
- Delavat, F., Miyazaki, R., Carraro, N., Pradervand, N. and van der Meer, J.R. (2017) The hidden life of integrative and conjugative elements. *FEMS Microbiol. Rev.*, **41**, 512–537.
- Wozniak, R.A. and Waldor, M.K. (2010) Integrative and conjugative elements: mosaic mobile genetic elements enabling dynamic lateral gene flow. *Nat. Rev. Microbiol.*, **8**, 552–563.
- Burrus, V. and Waldor, M.K. (2004) Shaping bacterial genomes with integrative and conjugative elements. *Res. Microbiol.*, **155**, 376–386.
- Beaber, J.W., Hochhut, B. and Waldor, M.K. (2004) SOS response promotes horizontal dissemination of antibiotic resistance genes. *Nature*, **427**, 72–74.
- Carraro, N., Richard, X., Sulser, S., Delavat, F., Mazza, C. and van der Meer, J.R. (2020) An analog to digital converter controls bistable transfer competence development of a widespread bacterial integrative and conjugative element. *Elife*, **9**, e57915.
- Achtung, J.M., Lee, C.A., Monson, R.E., Lehman, A.P. and Grossman, A.D. (2005) Regulation of a *Bacillus subtilis* mobile genetic element by intercellular signaling and the global DNA damage response. *Proc. Natl. Acad. Sci. U.S.A.*, **102**, 12554–12559.
- Reinhard, F., Miyazaki, R., Pradervand, N. and van der Meer, J.R. (2013) Cell differentiation to “mating bodies” induced by an integrating and conjugative element in free-living bacteria. *Curr. Biol.*, **23**, 255–259.
- Minoia, M., Gaillard, M., Reinhard, F., Stojanov, M., Sentschilo, V. and van der Meer, J.R. (2008) Stochasticity and bistability in horizontal transfer control of a genomic island in *Pseudomonas*. *Proc. Natl. Acad. Sci. U.S.A.*, **105**, 20792–20797.
- Delavat, F., Moritz, R. and van der Meer, J.R. (2019) Transient replication in specialized cells favors transfer of an integrative and conjugative element. *Mbio*, **10**, e01133-19.
- Fronzes, R., Christie, P.J. and Waksman, G. (2009) The structural biology of type IV secretion systems. *Nat. Rev. Microbiol.*, **7**, 703–714.
- Costa, T.R.D., Harb, L., Khara, P., Zeng, L., Hu, B. and Christie, P.J. (2021) Type IV secretion systems: advances in structure, function, and activation. *Mol. Microbiol.*, **115**, 436–452.
- Guglielmini, J., Neron, B., Abby, S.S., Garcillan-Barcia, M.P., de la Cruz, F. and Rocha, E.P. (2014) Key components of the eight classes of type IV secretion systems involved in bacterial conjugation or protein secretion. *Nucleic Acids Res.*, **42**, 5715–5727.

15. Juhas, M., Crook, D.W., Dimopoulou, I.D., Lunter, G., Harding, R.M., Ferguson, D.J. and Hood, D.W. (2007) Novel type IV secretion system involved in propagation of genomic islands. *J. Bacteriol.*, **189**, 761–771.
16. Sentchilo, V., Czechowska, K., Pradervand, N., Minoia, M., Miyazaki, R. and van der Meer, J.R. (2009) Intracellular excision and reintegration dynamics of the ICE_{clc} genomic island of *Pseudomonas knackmussii* sp. Strain B13. *Mol. Microbiol.*, **72**, 1293–1306.
17. Miyazaki, R., Bertelli, C., Benaglio, P., Canton, J., De Coi, N., Gharib, W.H., Gjoksi, B., Goesmann, A., Greub, G., Harshman, K. et al. (2015) Comparative genome analysis of *Pseudomonas knackmussii* B13, the first bacterium known to degrade chloroaromatic compounds. *Environ. Microbiol.*, **17**, 91–104.
18. Sentchilo, V., Zehnder, A.J. and van der Meer, J.R. (2003) Characterization of two alternative promoters for integrase expression in the *clc* genomic island of *Pseudomonas* sp. Strain B13. *Mol. Microbiol.*, **49**, 93–104.
19. Miyazaki, R. and van der Meer, J.R. (2011) A dual functional origin of transfer in the ICE_{clc} genomic island of *Pseudomonas knackmussii* B13. *Mol. Microbiol.*, **79**, 743–758.
20. Gaillard, M., Pradervand, N., Minoia, M., Sentchilo, V., Johnson, D.R. and van der Meer, J.R. (2010) Transcriptome analysis of the mobile genome *iceclc* in *Pseudomonas knackmussii* B13. *BMC Microbiol.*, **10**, 153.
21. Sulser, S., Vucicevic, A., Bellini, V., Moritz, R., Delavat, F., Sentchilo, V., Carraro, N. and van der Meer, J.R. (2022) A bistable prokaryotic differentiation system underlying development of conjugative transfer competence. *PLoS Genet.*, **18**, e1010286.
22. Jumper, J., Evans, R., Pritzel, A., Green, T., Figurnov, M., Ronneberger, O., Tunyasuvunakool, K., Bates, R., Zidek, A., Potapenko, A. et al. (2021) Highly accurate protein structure prediction with AlphaFold. *Nature*, **596**, 583–589.
23. Kelley, L.A., Mezulis, S., Yates, C.M., Wass, M.N. and Sternberg, M.J. (2015) The Phyre2 web portal for protein modeling, prediction and analysis. *Nat. Protoc.*, **10**, 845–858.
24. Hu, B., Khara, P. and Christie, P.J. (2019) Structural bases for F plasmid conjugation and F pilus biogenesis in *Escherichia coli*. *Proc. Natl. Acad. Sci. U.S.A.*, **116**, 14222–14227.
25. Aguilar, J., Zupan, J., Cameron, T.A. and Zambryski, P.C. (2010) *Agrobacterium* type IV secretion system and its substrates form helical arrays around the circumference of virulence-induced cells. *Proc. Natl. Acad. Sci. U.S.A.*, **107**, 3758–3763.
26. Ghosal, D., Jeong, K.C., Chang, Y.W., Gyore, J., Teng, L., Gardner, A., Vogel, J.P. and Jensen, G.J. (2019) Molecular architecture, polar targeting and biogenesis of the *Legionella* Dot/Icm T4SS. *Nat. Microbiol.*, **4**, 1173–1182.
27. Park, D., Chetrit, D., Hu, B., Roy, C.R. and Liu, J. (2020) Analysis of dot/Icm type IVB secretion system subassemblies by cryoelectron tomography reveals conformational changes induced by DotB binding. *Mbio*, **11**, e03328-19.
28. Gerhardt, P., Murray, R.G.E., Costilow, R.N., Nester, E.W., Wood, W.A., Krieg, N.R. and Briggs Phillips, G. (eds). (1981) In: *Manual of methods for general bacteriology*. American Society for Microbiology, Washington, D.C.
29. Gaillard, M., Vallaeyts, T., Vorhölter, F.J., Minoia, M., Werlen, C., Sentchilo, V., Pühler, A. and van der Meer, J.R. (2006) The *clc* element of *Pseudomonas* sp. strain B13, a genomic island with various catabolic properties. *J. Bacteriol.*, **188**, 1999–2013.
30. Martinez-Garcia, E. and de Lorenzo, V. (2011) Engineering multiple genomic deletions in gram-negative bacteria: analysis of the multi-resistant antibiotic profile of *Pseudomonas putida* KT2440. *Environ. Microbiol.*, **13**, 2702–2716.
31. Martinez-Garcia, E., Calles, B., Arevalo-Rodriguez, M. and de Lorenzo, V. (2011) pBAM1: an all-synthetic genetic tool for analysis and construction of complex bacterial phenotypes. *BMC Microbiol.*, **11**, 38.
32. Miyazaki, R., Minoia, M., Pradervand, N., Sulser, S., Reinhard, F. and van der Meer, J.R. (2012) Cellular variability of RpoS expression underlies subpopulation activation of an integrative and conjugative element. *PLoS Genet.*, **8**, e1002818.
33. Grote, A., Hiller, K., Scheer, M., Munch, R., Nortemann, B., Hempel, D.C. and Jahn, D. (2005) JCat: a novel tool to adapt codon usage of a target gene to its potential expression host. *Nucleic Acids Res.*, **33**, W526–W531.
34. Altschul, S.F., Gish, W., Miller, W., Myers, E.W. and Lipman, D.J. (1990) Basic local alignment search tool. *J. Mol. Biol.*, **215**, 403–410.
35. Mistry, J., Chuguransky, S., Williams, L., Qureshi, M., Salazar, G.A., Sonnhammer, E.L.L., Tosatto, S.C.E., Paladin, L., Raj, S., Richardson, L.J. et al. (2021) Pfam: the protein families database in 2021. *Nucleic Acids Res.*, **49**, D412–D419.
36. Holm, L. (2020) DALI and the persistence of protein shape. *Protein Sci.*, **29**, 128–140.
37. Krogh, A., Larsson, B., von Heijne, G. and Sonnhammer, E.L. (2001) Predicting transmembrane protein topology with a hidden Markov model: application to complete genomes. *J. Mol. Biol.*, **305**, 567–580.
38. Nielsen, H., Engelbrecht, J., Brunak, S. and von Heijne, G. (1997) A neural network method for identification of prokaryotic and eukaryotic signal peptides and prediction of their cleavage sites. *Int. J. Neural Syst.*, **8**, 581–599.
39. Krissinel, E. and Henrick, K. (2004) Secondary-structure matching (SSM), a new tool for fast protein structure alignment in three dimensions. *Acta. Crystallogr. D Biol. Crystallogr.*, **60**, 2256–2268.
40. Stylianidou, S., Brennan, C., Nissen, S.B., Kuwada, N.J. and Wiggins, P.A. (2016) SuperSegger: robust image segmentation, analysis and lineage tracking of bacterial cells. *Mol. Microbiol.*, **102**, 690–700.
41. Reinhard, F. and van der Meer, J.R. (2013) Improved statistical analysis of low abundance phenomena in bimodal bacterial populations. *PLoS One*, **8**, e78288.
42. Nakano, N., Kubori, T., Kinoshita, M., Imada, K. and Nagai, H. (2010) Crystal structure of *Legionella* DotD: insights into the relationship between type IVB and type II/III secretion systems. *PLoS Pathog.*, **6**, e1001129.
43. Durie, C.L., Sheedlo, M.J., Chung, J.M., Byrne, B.G., Su, M., Knight, T., Swanson, M., Lacy, D.B. and Ohi, M.D. (2020) Structural analysis of the *Legionella pneumophila* dot/icm type IV secretion system core complex. *Elife*, **9**, e59530.
44. Moore, D., Maneewannakul, K., Maneewannakul, S., Wu, J.H., Ippen-Ihler, K. and Bradley, D.E. (1990) Characterization of the F-plasmid conjugative transfer gene *traU*. *J. Bacteriol.*, **172**, 4263–4270.
45. Chlebek, J.L., Hughes, H.Q., Ratkiewicz, A.S., Rayyan, R., Wang, J.C., Herrin, B.E., Dalia, T.N., Biaisi, N. and Dalia, A.B. (2019) PilT and PilU are homohexameric ATPases that coordinate to retract type IVa pili. *PLoS Genet.*, **15**, e1008448.
46. Aguilar, J., Cameron, T.A., Zupan, J. and Zambryski, P. (2011) Membrane and core periplasmic *agrobacterium tumefaciens* virulence type IV secretion system components localize to multiple sites around the bacterial perimeter during lateral attachment to plant cells. *Mbio*, **2**, e00218-11.
47. Delavat, F., Mitri, S., Pelet, S. and van der Meer, J.R. (2016) Highly variable individual donor cell fates characterize robust horizontal gene transfer of an integrative and conjugative element. *Proc. Natl. Acad. Sci. U.S.A.*, **113**, E3375–E3383.
48. Christie, P.J., Atmakuri, K., Krishnamoorthy, V., Jakubowski, S. and Cascales, E. (2005) Biogenesis, architecture, and function of bacterial type IV secretion systems. *Annu. Rev. Microbiol.*, **59**, 451–485.
49. Kubori, T. and Nagai, H. (2016) The type IVB secretion system: an enigmatic chimera. *Curr. Opin. Microbiol.*, **29**, 22–29.
50. Chetrit, D., Hu, B., Christie, P.J., Roy, C.R. and Liu, J. (2018) A unique cytoplasmic ATPase complex defines the *Legionella pneumophila* type IV secretion channel. *Nat. Microbiol.*, **3**, 678–686.
51. Ward, D.V., Draper, O., Zupan, J.R. and Zambryski, P.C. (2002) Peptide linkage mapping of the *Agrobacterium tumefaciens* vir-encoded type IV secretion system reveals protein subassemblies. *Proc. Natl. Acad. Sci. U.S.A.*, **99**, 11493–11500.
52. Yuan, Q., Carle, A., Gao, C., Sivanesan, D., Aly, K.A., Hoppner, C., Krall, L., Domke, N. and Baron, C. (2005) Identification of the VirB4–VirB8–VirB5–VirB2 pilus assembly sequence of type IV secretion systems. *J. Biol. Chem.*, **280**, 26349–26359.
53. Mossey, P., Hudacek, A. and Das, A. (2010) *Agrobacterium tumefaciens* type IV secretion protein VirB3 is an inner membrane protein and requires VirB4, VirB7, and VirB8 for stabilization. *J. Bacteriol.*, **192**, 2830–2838.
54. Jones, A.L., Shirasu, K. and Kado, C.I. (1994) The product of the *virB4* gene of *Agrobacterium tumefaciens* promotes accumulation of VirB3 protein. *J. Bacteriol.*, **176**, 5255–5261.

55. Jakubowski,S.J., Krishnamoorthy,V., Cascales,E. and Christie,P.J. (2004) *Agrobacterium tumefaciens* VirB6 domains direct the ordered export of a DNA substrate through a type IV secretion system. *J. Mol. Biol.*, **341**, 961–977.
56. Casu,B., Mary,C., Sverzhinsky,A., Fouillen,A., Nanci,A. and Baron,C. (2018) VirB8 homolog TraE from plasmid pKM101 forms a hexameric ring structure and interacts with the VirB6 homolog TraD. *Proc. Natl. Acad. Sci. U.S.A.*, **115**, 5950–5955.
57. Matilla,I., Alfonso,C., Rivas,G., Bolt,E.L., de la Cruz,F. and Cabezón,E. (2010) The conjugative DNA translocase TrwB is a structure-specific DNA-binding protein. *J. Biol. Chem.*, **285**, 17537–17544.
58. Redzej,A., Ukleja,M., Connery,S., Trokter,M., Felisberto-Rodrigues,C., Cryar,A., Thalassinou,K., Hayward,R.D., Orlova,E.V. and Waksman,G. (2017) Structure of a VirD4 coupling protein bound to a VirB type IV secretion machinery. *EMBO J.*, **36**, 3080–3095.
59. Cascales,E. and Christie,P.J. (2004) *Agrobacterium* VirB10, an ATP energy sensor required for type IV secretion. *Proc. Natl. Acad. Sci. U.S.A.*, **101**, 17228–17233.
60. Craig,L., Forest,K.T. and Maier,B. (2019) Type IV pili: dynamics, biophysics and functional consequences. *Nat. Rev. Microbiol.*, **17**, 429–440.
61. Hoppner,C., Liu,Z., Domke,N., Binns,A.N. and Baron,C. (2004) VirB1 orthologs from *Brucella suis* and pKM101 complement defects of the lytic transglycosylase required for efficient type IV secretion from *Agrobacterium tumefaciens*. *J. Bacteriol.*, **186**, 1415–1422.
62. Mushegian,A.R., Fullner,K.J., Koonin,E.V. and Nester,E.W. (1996) A family of lysozyme-like virulence factors in bacterial pathogens of plants and animals. *Proc. Natl. Acad. Sci. U.S.A.*, **93**, 7321–7326.
63. Elton,T.C., Holland,S.J., Frost,L.S. and Hazes,B. (2005) F-like type IV secretion systems encode proteins with thioredoxin folds that are putative DsbC homologues. *J. Bacteriol.*, **187**, 8267–8277.
64. Saveson,C.J. and Lovett,S.T. (1999) Tandem repeat recombination induced by replication fork defects in *Escherichia coli* requires a novel factor, RadC. *Genetics*, **152**, 5–13.
65. Redfield,R.J., Cameron,A.D., Qian,Q., Hinds,J., Ali,T.R., Kroll,J.S. and Langford,P.R. (2005) A novel CRP-dependent regulon controls expression of competence genes in *Haemophilus influenzae*. *J. Mol. Biol.*, **347**, 735–747.
66. Berka,R.M., Hahn,J., Albano,M., Draskovic,I., Persuh,M., Cui,X., Sloma,A., Widner,W. and Dubnau,D. (2002) Microarray analysis of the *Bacillus subtilis* K-state: genome-wide expression changes dependent on ComK. *Mol. Microbiol.*, **43**, 1331–1345.
67. Rimini,R., Jansson,B., Feger,G., Roberts,T.C., de Francesco,M., Gozzi,A., Faggioni,F., Domenici,E., Wallace,D.M., Frandsen,N. *et al.* (2000) Global analysis of transcription kinetics during competence development in *Streptococcus pneumoniae* using high density DNA arrays. *Mol. Microbiol.*, **36**, 1279–1292.
68. Ogura,M., Yamaguchi,H., Kobayashi,K., Ogasawara,N., Fujita,Y. and Tanaka,T. (2002) Whole-genome analysis of genes regulated by the *Bacillus subtilis* competence transcription factor ComK. *J. Bacteriol.*, **184**, 2344–2351.
69. Attaiech,L., Granadel,C., Claverys,J.P. and Martin,B. (2008) RadC, a misleading name? *J. Bacteriol.*, **190**, 5729–5732.
70. Hong,J.S., Yoon,E.J., Lee,H., Jeong,S.H. and Lee,K. (2016) Clonal dissemination of *Pseudomonas aeruginosa* sequence type 235 isolates carrying blaIMP-6 and emergence of blaGES-24 and blaIMP-10 on novel genomic islands PAGI-15 and -16 in South Korea. *Antimicrob. Agents Chemother.*, **60**, 7216–7223.
71. Roy Chowdhury,P., Scott,M., Worden,P., Huntington,P., Hudson,B., Karagiannis,T., Charles,I.G. and Djordjevic,S.P. (2016) Genomic islands 1 and 2 play key roles in the evolution of extensively drug-resistant ST235 isolates of *Pseudomonas aeruginosa*. *Open Biol.*, **6**, 150175.